STUDIES OF COMPACT EXTRAGALACTIC RADIO SOURCES

Thesis by

Roger Paul Linfield

In Partial Fulfillment of the Requirements

for the Degree of

Doctor of Philosophy

California Institute of Technology

Pasadena, California

1981

(Submitted April 28, 1981)

ACKNOWLEDGEMENTS

Marshall Cohen introduced me to the world of radio astronomy. Through clever manipulation he ensured that I had experienced all aspects of VLBI before embarking on the project of Chapter 1. He helped me through numerous potential disasters along the way, and made many lengthy and detailed comments on early drafts of the paper.

Roger Blandford suggested the project that comprises Chapter 3, and patiently helped me along as I stumbled towards its conclusion. He made numerous helpful suggestions, and tactfully pointed out my errors. He provided much help in my work on Chapter 2 as well. I had many useful discussions with Tony Readhead in the course of my research, and he read through several drafts of Chapters 1 and 3.

Dave Fort readily agreed to operate the telescope at ARO for my experiment in December, 1978, in return for observing help at Owens Valley that he has not yet demanded. Harry Hardebeck was of great assistance during my many observing runs at Owens Valley. My special thanks go to the person responsible for the stereo in the VLBI correlator room.

Life would have been very different without my fellow students. Conversations with John Hoessel provided a frequent, and needed, escape from the routine of work. From John Huchra I heard many lively, entertaining (and incorrect) tales. Doug Rabin helped humble me during my first few months here. Richard Simon provided a useful second opinion on many of my data analysis schemes, and showed himself to be a true friend by fixing me up with his sister-in-law.

Finally, I wish to thank various climbing partners for accompanying me on my weekend trips to the mountains and desert, and on my occasional nighttime escapades up the sides of campus buildings. These people helped me preserve my sanity.

ABSTRACT

Three studies of compact, extragalactic radio sources are presented.

In the first, VLBI maps are presented of the nuclear cores of four radio galaxies which have large symmetric radio lobes: 3C 111, 3C 390.3, Cyg A, and 0055+30. Each source contains a nuclear jet having a scale of 1 pc, but no counterjets are seen. The jets in 3C 111 and 0055+30 point directly at the outer radio lobes, but in 3C 390.3 and Cyg A the jets are pointed from 4 to 6 degrees away from the lobes.

The implications of the maps and models of these sources are considered in the second study. It is concluded that in all four cases, the observed asymmetry reflects an intrinsic asymmetry on a msec scale. The minimum pressure in the four jets is calculated, and it is concluded that the jet in Cyg A is very unlikely to be confined by gas pressure.

In the third study, an attempt is made to explain the structure of compact radio sources with a precession-like motion of a relativistic jet. It is found that the curvature of these sources can be readily explained in this way. In addition, the knots which are often revealed by VLBI observations arise naturally in such a model. The main

problem with the model is that it cannot by itself explain the arcsecond structure of asymmetric radio sources.

TABLE OF CONTENTS

INTRODUCTION

After the discovery by Baade and Minkowski (1954) that the powerful radio source Cygnus A is coincident with a distant ($z \approx .05$) galaxy, it became clear that a large fraction of the cataloged radio sources (from low frequency surveys) were extragalactic. As higher resolution observations became available, initially from Owens Valley and Jodrell Bank, many of these sources were observed to be double in nature, consisting of two large (a few to many kpc) unconnected lobes (Miley 1980).

As higher frequency interferometers were developed, many (or most) of these 'double' sources were found to contain a third component, situated approximately midway between the other two. These central components were generally weaker than the other two at centimeter wavelengths. They were unresolved with the available resolution (a few arcseconds) and had flat or rising spectra ($\alpha \gtrsim 0$, where $S \propto \nu^{\alpha}$), in contrast to the steep spectra (typically $-1.2 < \alpha < -.5$) of the two lobes. These central components, coincident with an optical galaxy or quasar, were the obvious source of energy for the lobes. In addition, calculations of synchrotron lifetimes in the brightest parts of the lobes made it clear that relativistic particles are being continuously supplied to the lobes. This supply

probably, but not certainly, takes the form of beams (or jets) of material from the core.

Observations of the central components are the obvious way of determining the existence of this energy pipeline. VLBI observations are capable of resolving these central components, but in the decade or so after VLBI first became available, its sensitivity was too low. In the late seventies, low noise cryogenic receivers were installed at several telescopes, allowing .5-1 Jy sources to be studied in detail by multi-station VLBI observations. Chapter 1 of this thesis reports on such observations of the central components of four 'double' radio galaxies, in all of which extensions, or jets, were found. The consequences of these observations are explored in Chapter 2, where questions such as the asymmetry and possible pressure confinement of these jets are dealt with.

Not all radio sources in low frequency surveys are double (or triple) in nature. A few were largely or entirely unresolved with early instruments. Higher frequency surveys revealed many more of these 'core' sources. They typically have $-.2<\alpha<.5$, much like the central components of 'double' sources. These sources are often very strong at high frequencies, and were the first objects to be studied with VLBI. Several of them (3C 273, 3C 279, 3C 345) were found to be double in nature on a msec scale. Observations at several epochs produced the astounding result that the two

components of the double were separating with an apparent velocity of more than twice the speed of light. Such 'superluminal' sources have received a great deal of subsequent study, much of it here at Caltech. My participation in this effort is reflected in co-authorship of five papers on the subject (Cohen et al 1977, Seielstad et al 1979, Pearson et al 1981, Cohen et al 1981, and Walker et al 1981). The following picture of 'core' sources in general, and superluminal sources in particular, has emerged (Kellermann and Pauliny-Toth 1981). A very small (<1 msec diameter), self-absorbed core has a one-sided jet emerging from it. This jet curves continuously through 25°-40° in PA, and often leads into a steep-spectrum, arcsecond jet, whose flux is a small fraction of the total source flux. In the 'superluminal' sources, knots are seen to move rectilinearly along the jet, away from the central, self-absorbed core. The early modeling of 3C 273, 3C 279, and 3C 345 as doubles was apparently possible only because of the existence of a bright knot in the jet, with a flux comparable to that of the core.

The best explanation for these 'core' sources seems to be that they consist of a jet pointing nearly at us (Readhead et al 1978). The apparent faster than light expansion can be explained in this way with jet speeds less than that of light. Apparent velocities as great as $\gamma\beta$ can be observed, depending upon the viewing angle. The observed large curvature is explained as an amplification (due to projection effects) of a slight intrinsic curvature.

In Chapter 3 of this thesis, a model of 'core' sources is presented. The hypothesized intrinsic jet curvature is produced by a precession-like motion of the base of the jet. The features of the sources produced by this model are compared to the features in real sources.

REFERENCES

Baade, W., and Minkowski, R. 1954, Ap. J., 119, 206.

Cohen, M. H., Kellermann, K. I., Shaffer, D. B., Linfield, R. P., Moffet, A. T., Romney, J. D., Seielstad, G. A., Pauliny-Toth, I. I. K., Preuss, E., Witzel, A., Schilizzi, R. T., and Geldzahler, B. J. 1977, Nature, 268, 405.

Cohen, M. H., Unwin, S. C., Simon, R. S., Seielstad, G. A., Pearson, T. J., Linfield, R. P., and Walker, R. C. 1981, Ap. J. (in press)

Kellermann, K. I., and Pauliny-Toth, I. I. K. 1981, A.R.A.A. (in press)

Miley, G. 1980, A.R.A.A., 18, 165.

Pearson, T. J., Cohen, M. H., Linfield, R. P., Readhead, A. C. S., Seielstad, G. A., Simon, R. S., Unwin, S. C., and Walker, R. C. 1981, Nature, 290, 365.

Readhead, A. C. S., Cohen, M. H., and Pearson, T. J. 1978, Nature, 276, 768.

Seielstad, G. A., Cohen, M. H., Linfield, R. P., Moffet, A. T., Romney, J. D., Schilizzi, R. T., and Shaffer, D. B. 1979, Ap. J., 229, 53.

Walker, R. C., Seielstad, G. A., Simon, R. S., Unwin, S .C., Cohen, M. H., Pearson, T. J., and Linfield, R. P. 1981 (submitted)

CHAPTER 1

VLBI OBSERVATIONS OF JETS IN DOUBLE RADIO GALAXIES

THE ASTROPHYSICAL JOURNAL, 244: 436–446, 1981 March 1

VLBI OBSERVATIONS OF JETS IN DOUBLE RADIO GALAXIES

ROGER LINFIELD
Owens Valley Radio Observatory, California Institute of Technology
Received 1980 June 30; accepted 1980 September 23

ABSTRACT

We have made VLBI maps of the nuclear cores of four radio galaxies which have large symmetric radio lobes: 3C 111, 3C 390.3, Cyg A, and 0055+30. Each source contains a nuclear jet having a scale of 1 pc, but no counterjets were seen. The jet in 3C 111 points within 1° of the brightest region (hot spot) of one of the outer lobes, but in 3C 390.3 and Cyg A the jets are pointed from 4° to 6° away from the hot spots. The large scale structure of 0055+30 exhibits a range of position angles; this range includes the position angle of our nuclear jet.

Subject headings: galaxies: nuclei — galaxies: structure — interferometry — radio sources: galaxies

I. INTRODUCTION

Most observed extragalactic radio sources fall into two classes (Readhead, Cohen, and Pearson 1978). In the first, most of the emission comes from a compact core coincident with the optical object, and the remainder is asymmetrically distributed on one side of the core. In the second, the emission is largely from regions a few arcsec to several arcmin in size, symmetrically located about the associated optical object, and there is sometimes a weak compact radio source associated with the optical object.

The compact components in both classes of objects have sizes on the order of milliseconds, making them good candidates for very long baseline interferometry (VLBI). The first class of objects (asymmetric sources) has been the best studied by VLBI, largely because the strongest sources are in this category. In contrast, the second class (symmetric sources), with much weaker compact components, has received relatively little attention from VLBI observers. Several papers (Broderick and Condon 1975; Walker *et al.* 1976; Preuss *et al.* 1977; Schilizzi 1976) have presented VLBI detections of compact cores in a number of these sources. More detailed observations have led to a map of one, NGC 6251 (Cohen and Readhead 1979), and models of two others, 3C 236 (Schilizzi *et al.* 1979) and 3C 111 (Pauliny-Toth *et al.* 1976).

In this paper the results of multi-station VLBI observations of the compact components of four radio galaxies with symmetric, large-scale structure are reported. Hybrid maps (Readhead and Wilkinson 1978) are presented for each source. A later paper will deal with interpretation of the results. The sources, their redshifts, and their linear scales on the sky (a value for H_0 of 50 km s^{-1} Mpc^{-1} has been assumed) are given in Table 1.

In this paper we use the term "jet" to describe the radio structures we observe, even when they are only elongated by a few beamwidths. We feel that this is justified, because our limited sensitivity and dynamic range allow us to follow the elongations for only a short distance from the core. (The data for 3C 111 has the highest signal-to-noise ratio, and the observed length of its jet is the greatest.)

II. OBSERVATIONS

All observations were made at 10.65 GHz, using left circular polarization. The telescopes involved were: the 100 m telescope of the Max Planck Institut für Radioastronomie (BONN), the 37 m telescope of the Northeast Radio Observatory Corporation (HSTK), the 43 m telescope of the National Radio Astronomy Observatory (NRAO), the 46 m telescope of the Algonquin Park Radio Observatory (ARO), the 26 m telescope of the Harvard Radio Astronomy Station (FDVS), and the 40 m telescope of the Owens Valley Radio Observatory (OVRO). Typical system temperatures and gains (in K Jy^{-1}) for each telescope are given in Table 2. The schedule of observations is listed in Table 3.

TABLE 1

REDSHIFTS AND LINEAR SCALES

Source	z	Scale (kpc/″)
0055+30	0.0167	0.48
3C 111	0.0485	1.4
3C 390.3	0.0561	1.6
Cyg A	0.0565	1.6

TABLE 2

TYPICAL PARAMETERS OF TELESCOPES AT 10.65 GHz

Station	Typical T_{sys}	K Jy^{-1}
BONN	80	1.28
HSTK	95	0.125
ARO	115	0.223
NRAO	120	0.270
FDVS	280	0.055
OVRO	80	0.223

TABLE 3

OBSERVING SCHEDULE

Source	1978.93	1979.44	1979.75
3C 111	HAGFO	BHGO	...
3C 390.3	HAGFO	...	BHO
Cyg A	HAGFO	BHGO	...
0055+30	HAGFO	BHGO	...

NOTE.—B = BONN, H = HSTK, A = ARO, G = NRAO, F = FDVS, and O = OVRO.

Data were recorded with the NRAO Mark II system (Clark 1973; Moran 1976) using a bandwidth of 1.8 MHz. Hydrogen maser frequency standards at each station allowed a coherent integration time of 6 minutes. In some cases the data were then averaged incoherently for 12 or 18 minutes.

III. DATA REDUCTION

The correlation coefficients were converted to correlated flux densities by the standard procedure (Cohen *et al.* 1975). One complication in the present case arises from the extended nature of the sources. This causes some flux from the outer lobes to be picked up by the beam of the telescope, so that the core flux cannot be measured with a single antenna. To overcome this difficulty, the flux of the central components of 0055+30 and 3C 111 at 10.69 GHz were measured with the Stanford 5 element interferometer[1] for the epochs 1978.93 and 1979.44. The flux of the central component of 3C 390.3 was measured for the epoch 1978.93, but not for 1979.75, because the Stanford telescope had been shut down. This telescope could not measure the central component of Cyg A because of the large flux from the outer lobes. Therefore, the core flux was assumed to be the same as the peak correlated flux on the shortest baseline.

Another complication arises from the low signal-to-noise ratio (S/N) of the data, particularly on baselines involving FDVS. This leads to two types of bias on the visibility amplitudes. These are discussed in the Appendix. Phases were not affected.

After the corrections for these biases had been applied, models of the brightness distribution, consisting of 2–4 Gaussian components, were fitted to the amplitudes and closure phases for each source. These models were then used as input to the hybrid mapping procedure described by Readhead and Wilkinson (1978). It was found that with sufficient effort in the model-fitting stage to get a good fit, the hybrid mapping procedure converged on the first or second iteration. The output of this procedure is a set of several hundred δ-functions, whose Fourier transform fits the observations. The maps shown below were obtained by convolving the δ-functions with an elliptical Gaussian which has the same FWHM as the synthesized DIRTY beam.

[1] The observations at 10.69 GHz were supported by the Department of Electrical Engineering at Stanford University.

IV. RESULTS

a) 3C 111

The central component is coincident with a magnitude 18 object (Longair and Gunn 1975) which was recently found to be a galaxy with a bright stellar nucleus (Gunn, private communication). It has a broad emission line spectrum with a redshift of 0.0485 (Sargent 1977), but little else is known about its optical properties because of heavy foreground obscuration ($b = -9°$).

The central component has a steeply inverted radio spectrum ($\alpha > 0$, where $S \sim \nu^{\alpha}$), which is strongly variable on a time scale of a few months (Wills 1975). In late 1974 or early 1975, a large outburst occurred in which the 90 GHz flux increased by a factor of 5. 3C 111 had the strongest central component of the four sources that we observed ($S_{10.6} = 1.85 \pm 0.1$ Jy in 1978.93 and $S_{10.6} = 1.54 \pm 0.05$ Jy in 1979.44). It was detected as an X-ray source by *HEAO 1* (Marshall *et al.* 1978).

On a larger scale, 3C 111 exhibits the classical triple structure, as shown in Figure 1 (Laing 1980). The NE lobe is more compact than the SW lobe (2″ versus 10″) and has a more pronounced low surface brightness tail extending inward toward the central component. A substantial amount of the flux comes from low surface brightness emission, distributed between the two heads.

Previous VLBI observations (Pauliny-Toth *et al.* 1976) were made with three long baselines just after the large outburst of 1975. They yielded a model consisting of two components separated by 0.6 ms in position angle (PA) 58°, with a 180° ambiguity due to the lack of phase information.

In 1978.93, we obtained very good data at all five stations, allowing an excellent hybrid map (Fig. 2) to be made. The fit of the δ-functions comprising this map to the data is shown in Figure 3. A long (6 ms) straight jet at PA 63° ± 3° points directly at the NE lobe. A bright extension near the core and two knots (at 4.1 and 6.0 ms from the core) stand out on the map (the outer knot shows up more prominently with a different choice of contour levels), but there is also a smooth component to the jet. The jet is very one-sided—the counterjet (if present) is at least 15 times weaker than the jet.

PA errors in this paper were determined by rotating the components of the model or map about the core and observing how much this rotation degrades the fit to the data. Rotation by the quoted values makes the model or map inconsistent with the data; we consider it very unlikely that our values for the PA could be off by this much. In Figure 4, the δ-functions from the map in Figure 2 have been rotated by +3° (our PA error for that map), and the resulting fit to the data is shown.

Wills (1975) proposed a model of the central source consisting of an optically thick, self-absorbed component ($\theta < 1$ ms) and an optically thin, straight spectrum component ($0\farcs2 < \theta < 3''$). Using the simultaneous observations with VLBI (resolution ~1 ms) and the Stanford interferometer (resolution ~20″), we conclude that 3C 111 has less than 0.16 ± 0.2 Jy in structure between 0″.01 and 3″ at 10.65 GHz (versus 0.8 Jy from the

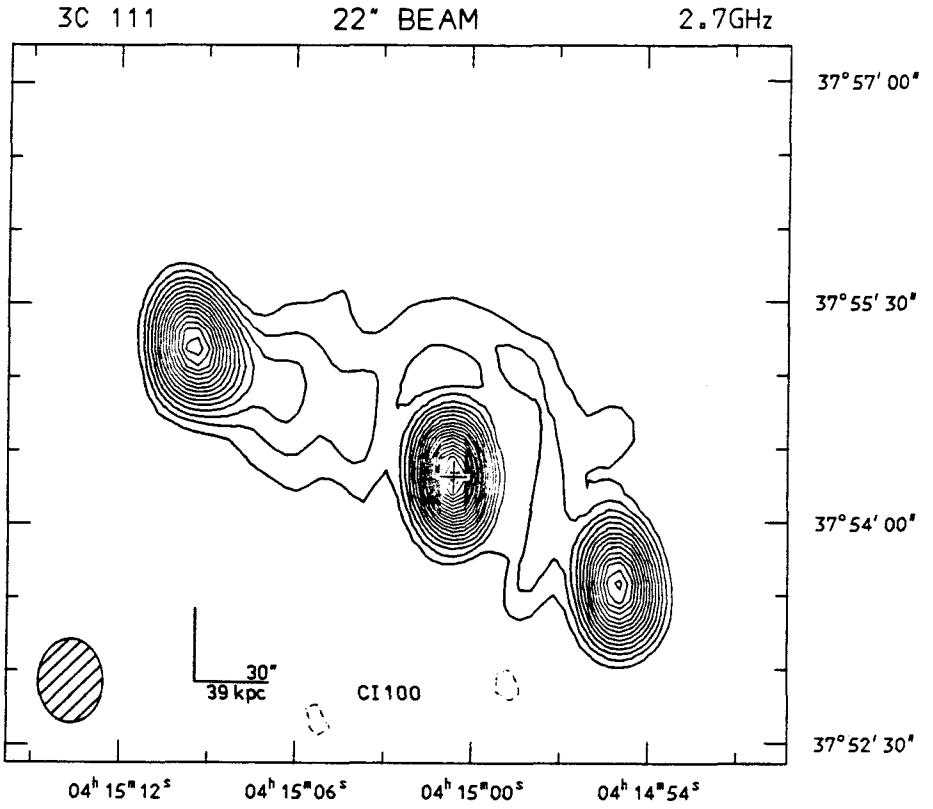

FIG. 1.—Map of 3C 111 at 2.7 GHz, made with the Cambridge 5 km telescope. The contour interval is 100 mJy per beam area. The cross marks the position of the associated optical galaxy. Included with the permission of Robert Laing.

model of Wills). Even in structure between 0".002 and 3" there is 0.57 ± 0.2 Jy, only marginally consistent with the extrapolated flux of Wills' optically thin component.

The map from the 1979.44 data has much poorer dynamic range, due to fewer baselines (6) and shorter tracks (an average of only 6 hours per baseline). The map shows an unresolved core and a short (1.5 ms smooth jet at PA 57° ± 9°. No knots are seen, but the knots shown in the 1978.93 map would be beyond the dynamic range of the 1979.44 data. The flux density dropped from 1.85 Jy to 1.54 Jy between 1978.93 and 1979.44, but we have no evidence for change in the structure during this interval. The lower 1979.44 flux presumably reflects a weakening of the unresolved core.

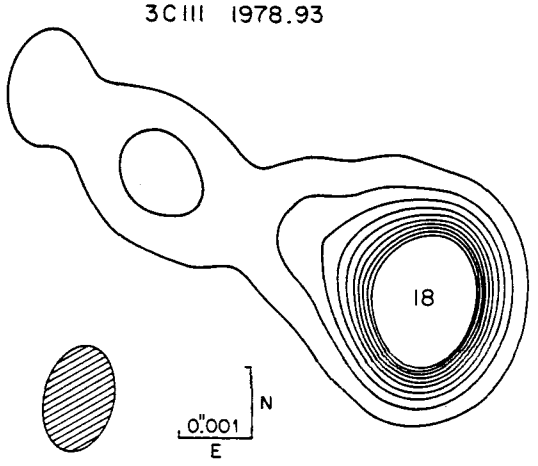

FIG. 2.—Hybrid map of 3C 111 from 1978.93, five-station VLBI observations. The contour interval is 2.8×10^8 K, with the lowest contour at 1.4×10^8 K. No negative contours appear at the -1.4×10^8 K level. Eighteen contours have been omitted in the unresolved core. The crosshatched ellipse shows the half-power beam.

b) 3C 390.3

3C 390.3 is in many ways similar to 3C 111. Its central component is coincident with a 12.8 mag galaxy (Wyndham 1966) with a redshift of 0.0561 (Sandage 1966). The galaxy has a very bright stellar nucleus; its spectrum has narrow H and forbidden lines, and very broad (10^4 km s^{-1}), asymmetric H lines, which are variable in both intensity and profile (Osterbrock, Koski, and Phillips 1976). The central component is a variable X-ray source (Marshall *et al.* 1978).

The central component has a lower radio luminosity than that of 3C 111, and its spectrum and behavior with time are consequently not as well known. Interferometer measurements (Bentley *et al.* 1975; Hargrave and McEllin 1975; and Stull *et al.* 1975) show that it has an inverted spectrum between 1.6 and 10 GHz, but apparently not as

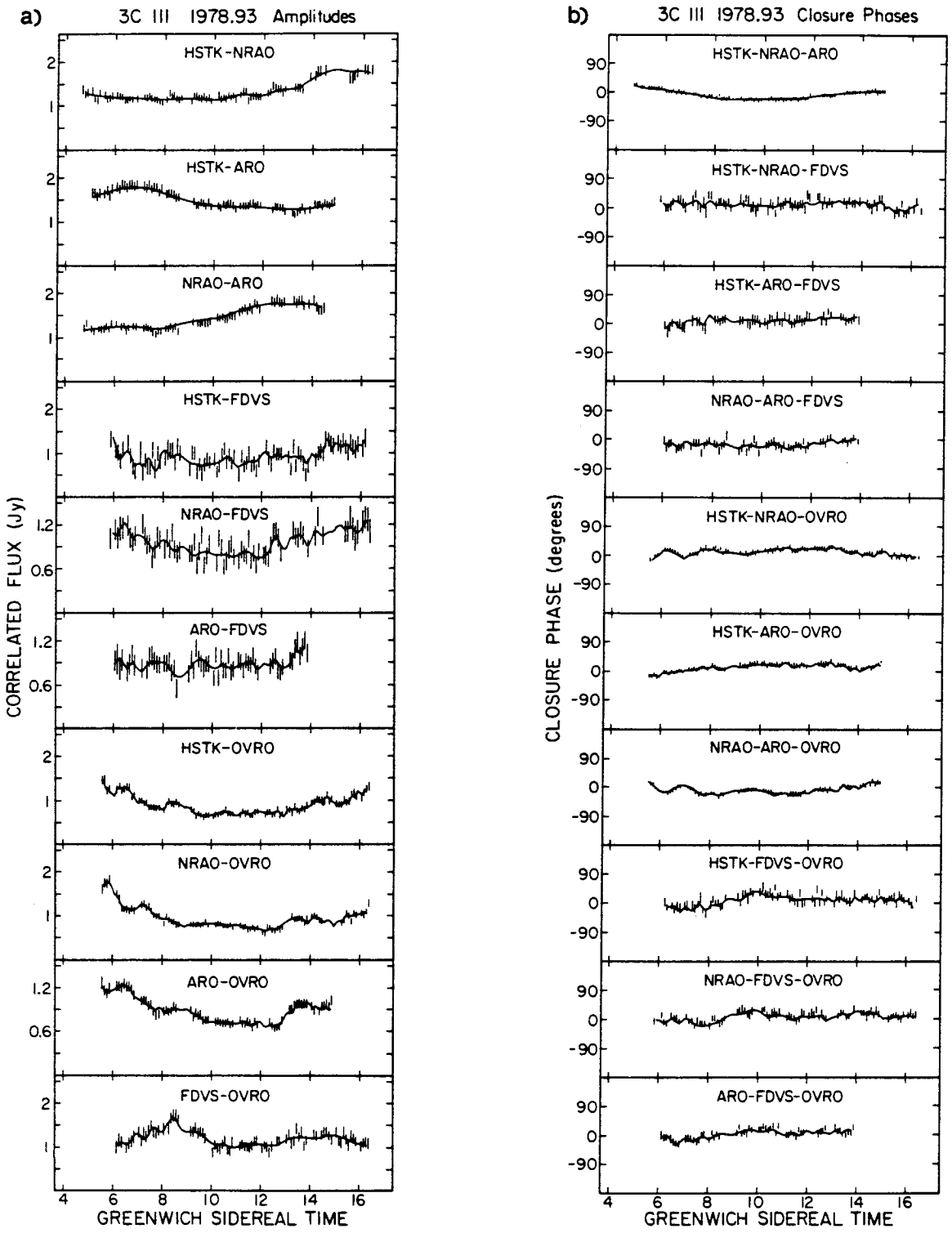

FIG. 3.—1978.93, 3C 111 data vs. GST. Solid lines correspond to the map in Fig. 2 (prior to convolution with the restoring beam). (*a*) Correlated flux densities. (*b*) Closure phases.

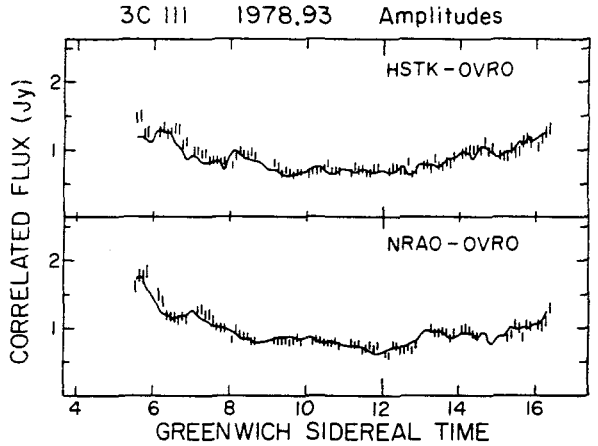

FIG. 4.—Fit of rotated 1978.93, 3C 111 map to data, showing degradation in the fit. The δ-functions of the map in Fig. 2 have been rotated by +3°.

steeply inverted as that of the central component in 3C 111.

All single-dish flux measurements are contaminated by contributions from the two extended lobes. Measurements with the Stanford five-element interferometer at 10.7 GHz in 1974 and 1978.93 provide the only positive evidence for variability (a decrease from 0.83 to 0.68 Jy in 4 years).

The arcmin scale structure of 3C 390.3 is shown in Figure 5 (Laing 1980). Unlike 3C 111, the central component and the two outer hot spots are very nearly in a line, at PA 144°–324°. Both the north and south lobes are resolved into two components by the 5 km telescope. The components of the north-preceding lobe are approximately 2″ in size, and are separated by 25″ in PA 117°; those of the south-following lobe are less than 1″ in size, and are separated by 2″.7 in PA 60°. The most compact component of the south-following lobe is at PA 144°.6. Both lobes, particularly the northern one, have some diffuse, steep spectrum emission, and there is some very low surface brightness emission extending from one lobe to the other.

In the 1978.93 observations of 3C 390.3, the OVRO data were very poor, and a map could not be made. A two-component model, with a very thin component

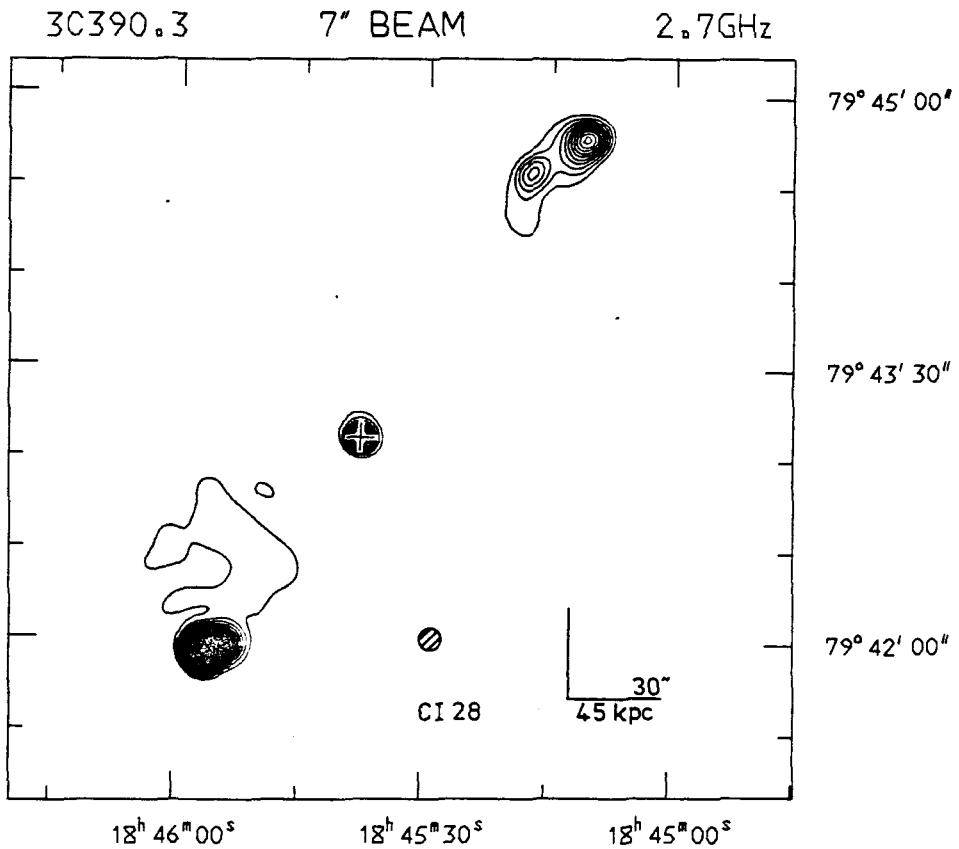

FIG. 5.—Map of 3C 390.3 at 2.7 GHz, made with the Cambridge 5 km telescope. The contour interval is 28 mJy per beam area. The cross marks the position of the associated optical galaxy. Included with the permission of Robert Laing.

TABLE 4

1979.75 3C 390.3 MODEL

Component	Flux	Displacement from First Component		FWHM Major Axis[a] (ms)	FWHM Minor Axis (ms)	PA
		d (ms)	PA			
1	.41	0.0	0.0	0.59	.14	−40°1
2	.06	0.53	146.3	0.26	.17	29.8
3	.03	1.22	141.1	1.1	.10	57.3

[a] Elliptical Gaussian components.

extended in PA 136° and a 50 mJy 2.4 ms FWHM halo, fit the data well. Because of pointing problems at OVRO, the evidence for the halo is weak, and the error in the PA is +12°.

In 1979.75 high quality data were obtained at BONN, HSTK, and OVRO. This allowed a good model (Table 4) and a good hybrid map (Fig. 6) to be made. Because only three stations were involved, the dynamic range is substantially worse than in maps of other sources from 1978.93. The data, with the fit from the map in Figure 6, are shown in Figure 7. The very large range of correlated flux on the BONN-OVRO baseline provides a tight constraint on the PA of the jet (140° ± 3°). Combining the results from the two epochs, we conclude that the jet is at PA 139°.5 ± 3° (i.e., misaligned with the SE lobe with a very high level of confidence).

c) *Cygnus A*

The central radio component was discovered in 1974 by Hargrave and Ryle (1974). It is coincident with a 15th mag cD galaxy with a prominent dust lane (Baade and Minkowski 1954). It has narrow (500 km s^{-1}) H and forbidden lines, but unlike 3C 111 and 3C 390.3, it has no very broad H lines (Osterbrock and Miller 1975). An extended (2′) X-ray source is centered on the galaxy (Fabbiano *et al.* 1979).

The outer radio lobes are very strong and the central component is difficult to detect, much less measure. For this reason its spectrum is only approximately known, and, although it would be expected to vary with time, there is no evidence for or against variability. Its spectrum appears to be slightly inverted between 1 and 100 GHz (Hobbs *et al.* 1978).

The arcsec scale structure of Cyg A is shown in Figure 8 (Hargrave and Ryle 1974). The line between the two outer hot spots of the SE lobe is at PA 109°; the hot spot of the NW lobe is at PA 290°. Higher resolution observations at 15 GHz (Hargrave and Ryle 1976) show that the NW hot

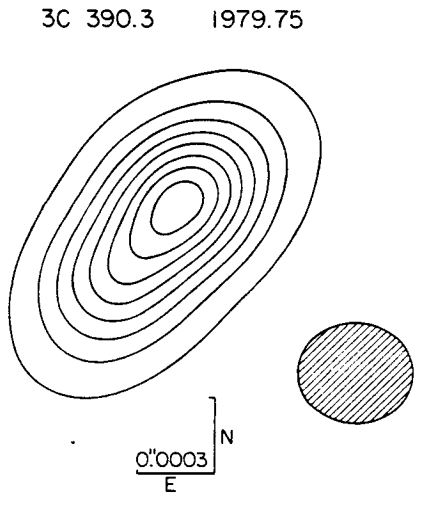

FIG. 6.—Hybrid map of 3C 390.3 from 1979.75, three-station VLBI observations. The contour interval is 16 × 10^8 K, with the lowest contour at 8 × 10^8 K. No negative contours appear at the −8 × 10^8 K level. The crosshatched ellipse shows the half-power beam.

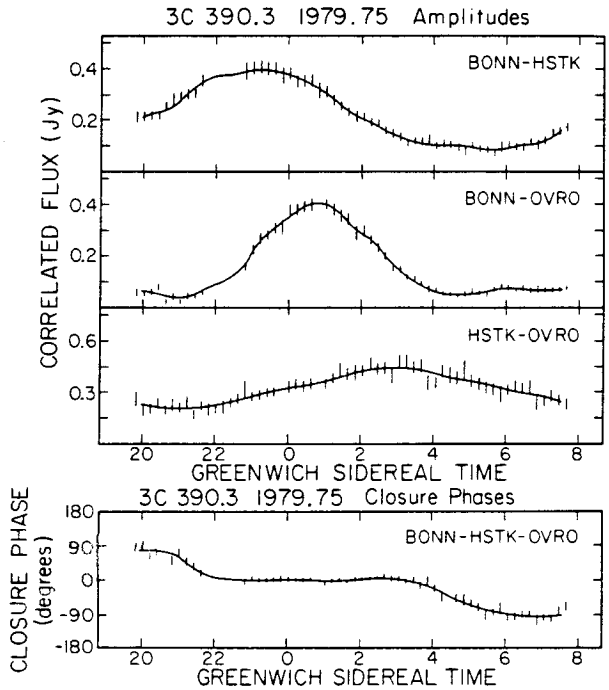

FIG. 7.—1979.75, 3C 390.3 correlated flux densities and closure phases vs. GST. Solid lines correspond to the map in Fig. 6 (prior to convolution with the restoring beam).

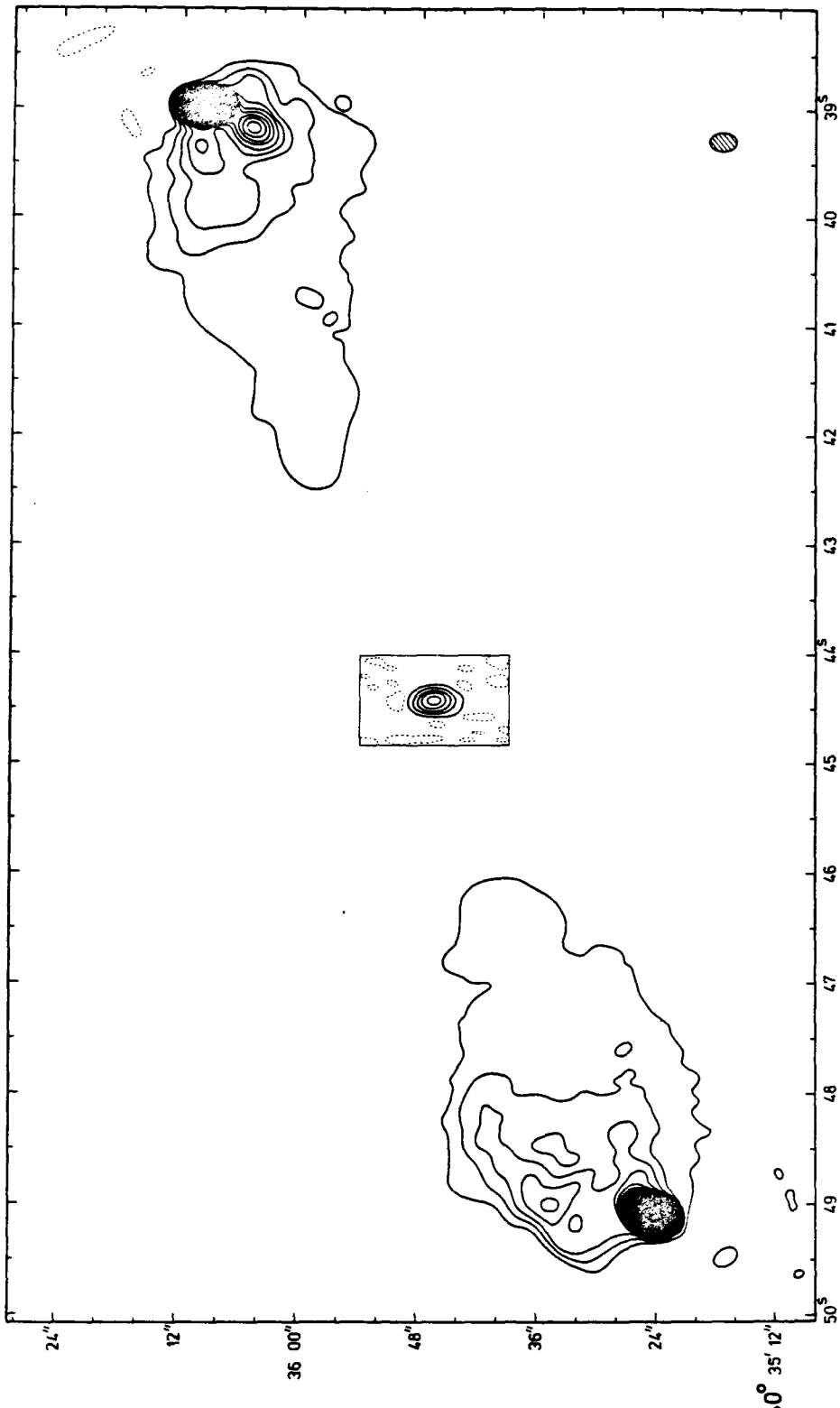

FIG. 8.—Map of Cyg A at 5 GHz, made by Hargrave and Ryle with the Cambridge 5 km telescope. Reproduced with the permission of Hargrave and Ryle and the Royal Astronomical Society.

spot breaks up into two components. The more compact of the two is at PA 288°9; the other is at PA 293°1. Both hot spots have very sharp (~ 0".5) leading edges; toward the galaxy the intensity of the lobes drops off more slowly, with low surface brightness tails reaching over halfway to the center. The sharpness of the leading edge of the SE hot spot led Hargrave and Ryle to conclude that the radio axis lies within 25° of the plane of the sky. Simkin (1977) has measured the rotation axis of the central galaxy, and finds it to be 6° from the plane of the sky and oriented at PA 116°.

Previous VLBI observations of Cyg A (Kellermann *et al.* 1975) had limited *U-V* coverage and indicated only that the central source was elongated and aligned approximately with the outer structure.

Our 1978.93 observations yielded the map shown in Figure 9. A straight jet emerges from the core at PA 284° (+5°, −4°). The jet is shorter than the jet in 3C 111; its PA is therefore not as well determined. The evidence for the knot 5 ms from the core is very good, but the exact distance is uncertain. There is no evidence for a counterjet; an upper limit of $\frac{1}{15}$ of the flux of the jet can be set to its flux.

The 1979.44 observations were plagued with calibration problems because BONN was mispointed for the last half of the track. To surmount these problems, a hybrid map (Fig. 10) was made using both closure phase and closure amplitudes, as described by Readhead *et al.* (1980). This eliminated systematic errors, but reduced the dynamic range. The map supplements the 1978.93 map in several ways. The new PA (283° + 5°, −6°) agrees with the previous PA. The higher resolution (BONN was not used in 1978.93) enables us to see that the jet is straight from 0.5 to 5 ms, and that it is less than 1 ms wide.

Combining the results from the two epochs, we get a PA of 283°5 (+4°, −3°5). This is 5°4 from the most compact component of the NW lobe—we consider it highly unlikely that our value for the PA could be off by this much.

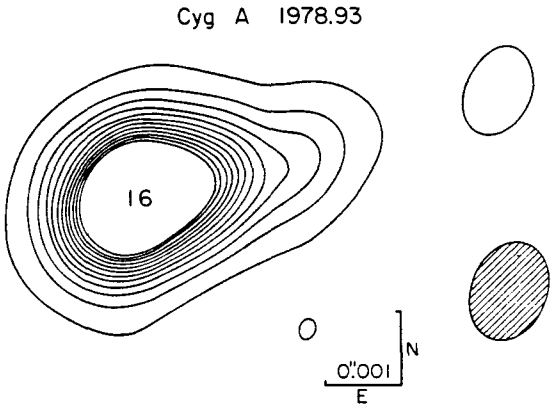

FIG. 9.—Hybrid map of Cyg A from 1978.93, five-station VLBI observations. The contour interval is 1.4×10^8 K, with the lowest contour at 0.7×10^8 K. No negative contours appear at the -0.7×10^8 K level. Sixteen contours have been omitted in the core. The crosshatched ellipse shows the half-power beam.

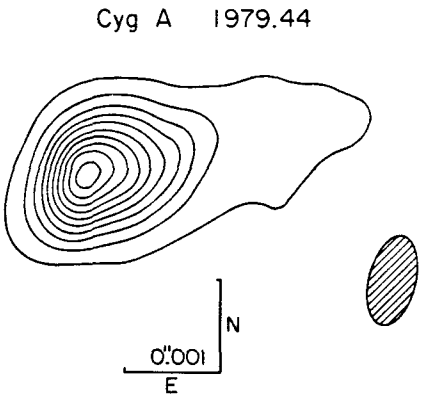

FIG. 10.—Hybrid map of Cyg A from 1979.44, four-station VLBI observations. The contour interval is 8×10^8 K, with the lowest contour at 4×10^8 K. No negative contours appear at the -4×10^8 K level. The crosshatched ellipse shows the half-power beam.

d) 0055+30

The central component of 0055+30 is coincident with a normal 12.5 mag elliptical galaxy (NGC 315), with no observed emission lines (Colla *et al.* 1975). It was not detected as an X-ray source by the 4*U* survey (Forman *et al.* 1978). This source has not been studied as well as the other three, and there is no evidence for or against variability. The spectrum of the central source is slightly inverted (Fanti *et al.* 1976).

The total angular extent on the sky of 0055+30 is almost 1° (Bridle *et al.* 1979). It has a *Z*-shaped symmetry, with both a jet and a counterjet (Fig. 11). Both the jet and counterjet wander in PA, with the PA of the jet varying roughly between 308° and 315°, with 311° the PA for the innermost structure seen with the VLA. The counterjet is a factor of 10 weaker than the jet and is more diffuse.

Our 1978.93 observations of 0055+30 produced the map shown in Figure 12. The PA of the jet is not constant, but varies from 306° near the core to 314° in the outer parts of the map. Maps without this curvature are also consistent with the data, although the fit is not as good; we are therefore not certain that the jet is curved. The outer PA (314°) is fairly well defined (±5°).

The 1979.44 observations yielded the map in Figure 13. The jet is straight (PA 314° ± 3°), but there may be a hint of the curvature present in the previous map (PA less than 314° at a distance of 2.5 ms from the core). The curvature seems to be more in the form of a kink in the jet than a systematic change with radius, as both the innermost region (~ 1.6 ms from the core on the 1979.44 map) and the outermost (4.5 ms on the 1978.93 map) have the same PA, with intermediate regions having a lower value.

No evidence for a counterjet is present on either of the maps. An upper limit of $\frac{1}{8}$ of the flux of the jet can be set for any counterjet with millisecond structure.

V. CONCLUSIONS

Four sources with symmetric, large-scale structure show one-sided jets on a millisecond scale. None show

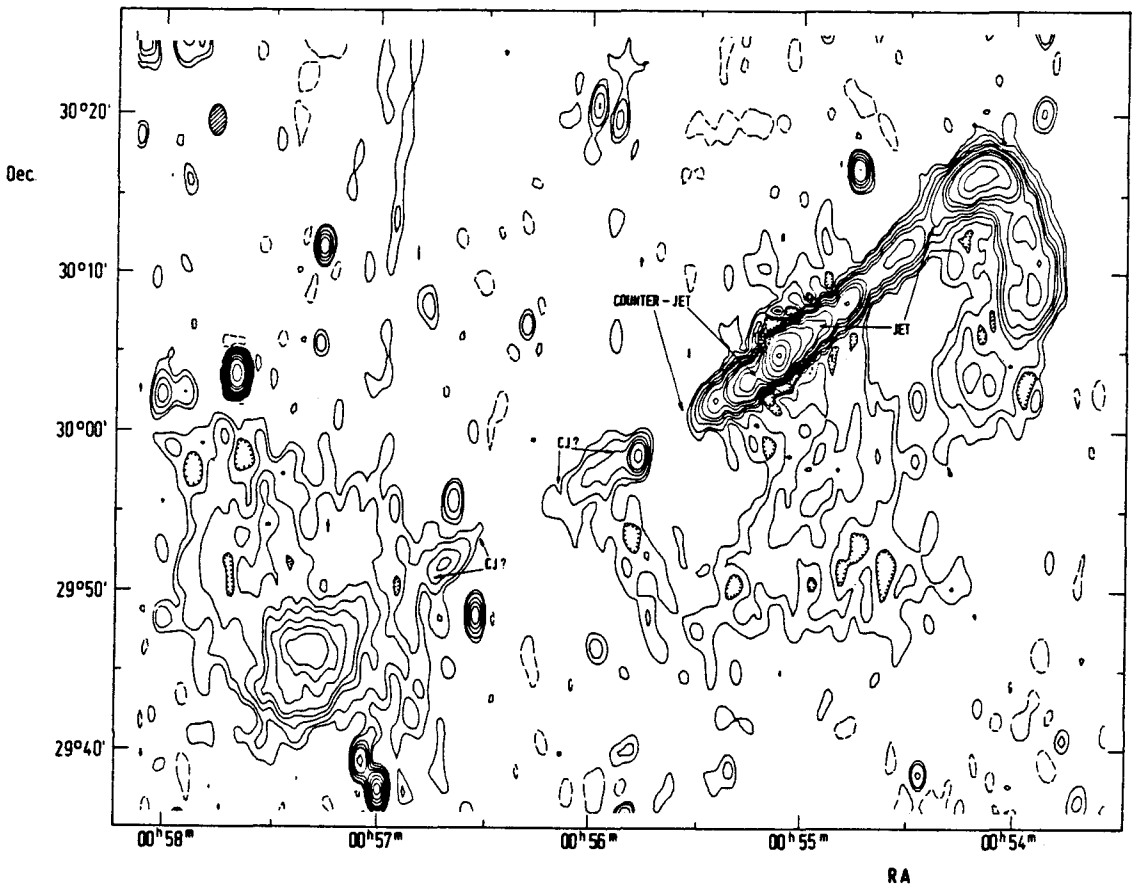

FIG. 11.—Contour map of 0055+30 at 610 MHz, made with the WSRT by Bridle *et al.* The cross is at the position of the optical galaxy. Reprinted with the permission of Bridle *et al.*

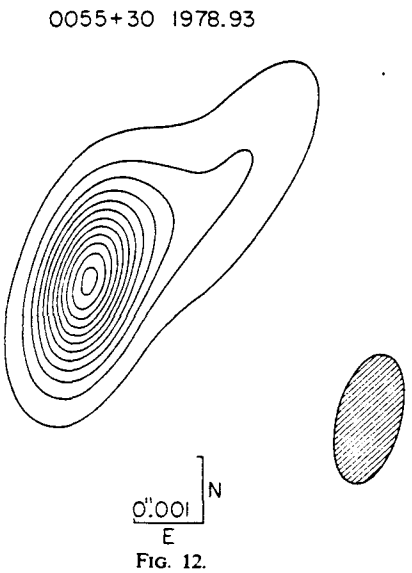

FIG. 12.

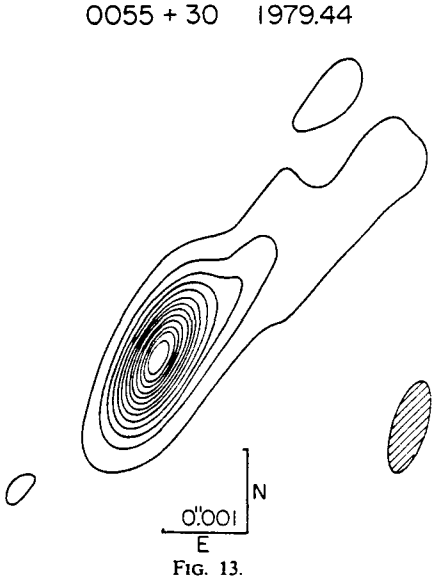

FIG. 13.

FIG. 12.—Hybrid map of 0055+30 from 1978.93, five-station VLBI observations. The contour interval is 2×10^8 K, with the lowest contour at 10^8 K. No negative contours appear at the -10^8 K level. The crosshatched ellipse shows the half-power beam.

FIG. 13.—Hybrid map of 0055+30 from 1979.44, four-station VLBI observations. The contour interval is 4×10^8 K, with the lowest contour at 2×10^8 K. No negative contours appear at the -2×10^8 K level. The crosshatched ellipse shows the half-power beam.

any systematic change of PA with distance from the core, in marked contrast to the asymmetric sources, which bend by 20° to 45° with increasing distance from the center (Readhead, Cohen, and Pearson 1978). The alignment between the jets and the outer lobes is quite good—within 8° in all cases. This is in agreement with the properties noted for symmetric sources. In two sources (3C 111 and 0055+30), the alignment is perfect (within the errors), but in the other two (3C 390.3 and Cyg A), the jet and outer lobe are misaligned by a few (4–6) degrees. This, together with a similar finding for NGC 6251 (Cohen and Readhead 1979), shows that in a substantial fraction of symmetric sources the jets are bent by a few degrees from core to outer lobe.

In three of the four sources (3C 111, 3C 390.3, and 0055+30), one of the two outer lobes is significantly more compact than the other. In all three, the nuclear jet points at or near the more compact lobe.

We thank D. Fort for operating the Algonquin Radio Observatory. J. Ball was of great help with the observations at Fort Davis. A. Rogers oversaw the operation of the Haystack Observatory at all three epochs. The flux measurements made with the Stanford five-element interferometer by R. N. Bracewell, W. Graf, and K. M. Price were very valuable. We thank R. Laing for an informative discussion and for allowing the use of his results in advance of publication. Through their heroic efforts, B. Geldzahler and R. Porcas kept the 1979.44 BONN observations from being cancelled. N. Renzetti and the Jet Propulsion Laboratory helped arrange for a Hydrogen Maser Frequency standard to be brought to OVRO for the 1979.44 observations when the existing one failed. M. Cohen, A. C. S. Readhead, and G. Purcell provided many helpful discussions. NRAO is operated by Associated Universities, Inc., under contract with the National Science Foundation. Radio Astronomy at Harvard Radio Astronomy Station is supported in part by the National Science Foundation. This research was supported in part by NSF grant AST 79-13249. Part of this work was done while the author was supported by an NSF predoctoral fellowship.

APPENDIX

BIAS IN THE VISIBILITY AMPLITUDES

I. THE DISTRIBUTION FUNCTION

Our fringe-fitting procedure yields fringe amplitudes which are biased, because we are detecting a sine wave in noise. The case of Gaussian noise and analysis with a one-dimensional Fourier transform is well known. The amplitudes have a Rice distribution (Purcell 1973; Moran 1973) with a mean larger than the true fringe visibility. However, we have used an iterative four-dimensional, nonlinear least-squares fitting procedure, and the probability distribution of the amplitudes has not yet been calculated. Instead, the bias has been determined empirically, by doing fringe-fitting on many scans at a wide range of coherent integration periods for each scan. The S/N for a given scan varies like

$$\mathrm{S/N} \sim \tau_{\mathrm{coh}}{}^{1/2}, \tag{1}$$

so this procedure produced amplitudes of many different S/N's for the same data. Applying this procedure to sources having very strong fringes, for which the bias should be negligible, gave the correction for loss of coherence with increasing integration time. Applying it to scans of different inherent S/N's showed that the bias is dependent only on S/N, not on integration time. Table 5 gives this bias, and the bias due to a Rice distribution, for several values of the S/N. Raw fringe amplitudes are too high and were corrected by division by the values in Table 5.

TABLE 5

FRINGE AMPLITUDE BIAS

S/N[a]	Rice Distribution Bias	Least Squares Procedure Bias
3	1.096	1.145
4	1.037	1.100
5	1.022	1.066
6	1.015	1.042
7	1.011	1.026
8	1.008	1.016
9	1.006	1.009
10	1.005	1.006

[a] The measured fringe amplitude divided by the noise level.

II. TRUNCATION

The second type of bias arises from the use of a S/N cutoff in the fringe-fitting procedure. (This cutoff is set at a level where the procedure begins to converge on noise a nonnegligible fraction of the time.) When the mean S/N of data is not too far above this cutoff, the low S/N tail of the distribution will be truncated. The mean of the resulting distribution will then be greater than the mean of the parent distribution. In order to correct the measured mean value for this effect, a particular parent distribution must be assumed. In this case it was chosen to be a Rice distribution. This is known to be wrong, as explained above, but the magnitude of this effect is relatively insensitive to the detailed nature of the parent distribution. This correction was only necessary on baselines to FDVS on the sources 0055+30, 3C 390.3, and Cyg A, and on the baseline BONN-OVRO for the source 3C 390.3 (at the visibility minimum only). On 3C 111 and on all other baselines, the S/N was high enough that truncation did not occur.

REFERENCES

Baade, W., and Minkowski, R. 1954, *Ap. J.*, **119**, 206.
Bentley, M., Haves, P., Spencer, R. E., and Stannard, D. 1975, *M.N.R.A.S.*, **173**, 93P.
Bridle, A. H., Davis, M. M., Fomalont, E. B., Willis, A. G., and Strom, R. G. 1979, *Ap. J. (Letters)*, **228**, L9.
Broderick, J. J., and Condon, J. J. 1975, *Ap. J.*, **202**, 596.
Clark, B. G. 1973, *Proc. IEEE*, **61**, 1242.
Cohen, M. H., *et al.* 1975, *Ap. J.*, **201**, 249.
Cohen, M. H., and Readhead, A. C. S. 1979, *Ap. J. (Letters)*, **233**, L101.
Colla, G., Fanti, C., Fanti, R., Gioia, I., Lari, C., Lequeux, J., Lucas, R., and Ulrich, M.-H. 1975, *Astr. Ap. Suppl.*, **20**, 1.
Fabbiano, G., Doxsey, R. E., Johnston, M., Schwartz, D. A., and Schwarz, J. 1979, *Ap. J. (Letters)*, **230**, L67.
Fanti, R., Lari, C., Spencer, R. E., and Warwick, R. S. 1976, *M.N.R.A.S.*, **174**, 5P.
Forman, W., Jones, C., Cominsky, L., Julien, P., Murray, S., Peters, G., Tananbaum, H., and Giacconi, R. 1978, *Ap. J. Suppl.*, **38**, 357.
Hargrave, P. J., and McEllin, M. 1975, *M.N.R.A.S.*, **173**, 37.
Hargrave, P. J., and Ryle, M. 1974, *M.N.R.A.S.*, **166**, 305.
———. 1976, *M.N.R.A.S.*, **175**, 481.
Hobbs, R. W., Maran, S. P., Kafatos, M., and Brown, L. W. 1978, *Ap. J. (Letters)*, **220**, L77.
Kellermann, K. I., Clark, B. G., Niell, A. E., and Shaffer, D. B. 1975, *Ap. J. (Letters)*, **197**, L113.
Laing, R. 1980, *M.N.R.A.S.*, in press.
Longair, M. S., and Gunn, J. E. 1975, *M.N.R.A.S.*, **170**, 121.
Marshall, F. E., Mushotzky, R. F., Boldt, E. A., Holt, S. S., Rothschild, R. F., and Serlemitsos, P. J. 1978, *Nature*, **275**, 624.
Moran, J. M. 1973, *Proc. IEEE*, **61**, 1236.
———. 1976, *Methods of Experimental Physics*, Vol. 12, Part C, ed. M. L. Meeks (New York: Academic Press), pp. 174–197.
Osterbrock, D. E., Koski, A. T., and Phillips, M. M. 1976, *Ap. J.*, **206**, 898.
Osterbrock, D. E., and Miller, J. S. 1975, *Ap. J.*, **197**, 535.
Pauliny-Toth, I. I. K., Preuss, E., Witzel, A., Kellermann, K. I., and Shaffer, D. B. 1976, *Astr. Ap.*, **52**, 471.
Preuss, E., Pauliny-Toth, I. I. K., Witzel, A., Kellermann, K. I., and Shaffer, D. B. 1977, *Astr. Ap.*, **54**, 297.
Purcell, G. H. 1973, Ph.D. thesis, California Institute of Technology.
Readhead, A. C. S., Cohen, M. H., and Pearson, T. J. 1978, *Nature*, **276**, 768.
Readhead, A. C. S., Walker, R. C., Pearson, T. J., and Cohen, M. H. 1980, in press.
Readhead, A. C. S., and Wilkinson, P. N. 1978, *Ap. J.*, **223**, 25.
Sandage, A. 1966, *Ap. J.*, **145**, 1.
Sargent, W. L. W. 1977, *Ap. J. (Letters)*, **212**, L105.
Schilizzi, R. T. 1976, *A.J.*, **81**, 946.
Schilizzi, R. T., Miley, G. K., van Ardenne, A., Baud, B., Bååth, L., Rönnäng, B. O., and Pauliny-Toth, I. I. K. 1979, *Astr. Ap.*, **77**, 1.
Simkin, S. M. 1977, *Ap. J.*, **217**, 45.
Stull, M. A., Price, K. M., D'Addario, L. R., Wernecke, S. J., Graf, W., and Grebenkemper, C. J. 1975, *A.J.*, **80**, 8.
Walker, R. C., Lo, K. Y., Burke, B. F., Johnston, K. J., and Moran, J. M. 1976, *Ap. J.*, **208**, 296.
Wills, B. J. 1975, *Ap. J. (Letters)*, **202**, L59.
Wyndham, J. D. 1966, *Ap. J.*, **144**, 459.

ROGER LINFIELD: Owens Valley Radio Observatory, 102-24, California Institute of Technology, Pasadena, CA 91125

CHAPTER 2

PARSEC-SCALE JETS IN DOUBLE RADIO GALAXIES. INTERPRETATIONS

I. INTRODUCTION

In Chapter 1, VLBI observations of the central components of 0055+30, 3C 111, 3C 390.3, and Cyg A were presented. This chapter deals with the interpretation of these observations.

In all four sources, a narrow, one-sided jet was seen emerging from the core. Within the dynamic range achieved by these observations, no counterjets were seen. The implications of this on the source geometry are considered in part II.

The most likely physical mechanism responsible for the radio emission from these sources is synchrotron radiation. If one assumes this to be the case, then the observed radiation properties can be converted to information on the physical conditions in the source. In part III, the observed brightness temperatures of the sources are compared with the range produced by synchrotron radiation. In addition, the magnetic field, internal energy, and pressure (assuming equipartition between the magnetic and particle energy densities) of the various components of these sources are calculated.

An important question in connection with jets in radio sources is whether or not they are confined by the gas pressure of the surrounding medium. The pressure calculated in part III places constraints on the proposed confining medium. Various physical considerations, combined with observations at X-ray wavelengths, allow additional constraints on

this medium; this is covered in part IV. Two alternatives to pressure confinement are briefly discussed.

II. IMPLICATIONS OF OBSERVED JET-COUNTERJET RATIOS

All four sources are more or less symmetrical on a large (arcsec-arcmin) scale. All four display approximate structural inversion symmetry (a pair of lobes in 3C 111, 3C 390.3, and Cyg A; a pair of scythe-shaped features in 0055+30) about the central component. That symmetry is broken in detail, however. The ratio of distances from the central components varies from 1.1 (Cyg A) to 2 (0055+30). The flux ratio also varies widely, from near unity in Cyg A to ~10 in 0055+30. (The exact value of the flux ratio is frequency dependent, and is difficult to determine due to the range of angular scales present in these sources.)

This large scale symmetry is in sharp contrast to the asymmetry observed on a msec scale. The observations in Chapter 1 showed extensions on only one side of the core in each source. Lower limits to the jet/counterjet flux of 8 (0055+30) and 15 (3C 111 and Cyg A) were established.

This msec asymmetry could be due to an intrinsic asymmetry between the jet and (presumed) counterjet. This seems likely in the case of 0055+30, where the flux of the arcsec and arcmin jet, and of the diffuse NW lobe, is 10 times that of the flux from the corresponding structures on the other side (the msec jet points in the same direction as the stronger of the two large scale ones). In 3C 111 and 3C 390.3 there is some evidence of jet/counterjet asymmetry in that in each source one of the two outer lobes is significantly more compact than the other. In both cases, the msec jet points at the more compact lobe. In Cyg A, however, the two lobes are very similar, with both being about equally luminous and equally compact. There is no a priori reason to suspect an intrinsic jet/counterjet asymmetry in this source.

An intrinsic asymmetry could take the form of a difference in time-averaged power, but this is unlikely except in 0055+30 because of similar lobe fluxes. It has been suggested by many people that jets become visible only when there are inefficiencies in the transport path. This is certainly possible, but the fact that the msec jets in 3C 111 and 3C 390.3 point towards the more compact lobe argues against it. A more acceptable explanation may be that the nuclear jet is one-sided, but intermittent, pointing first towards one lobe and then the other. This is in agreement with recent MTRLI observations (Lonsdale 1981). However, if this is a common situation, the switching time must be very long ($>10^6$ yr) for some sources (e.g. NGC 315 and NGC 6251).

If the jets are intrinsically similar, their very different observed luminosities could be due to a non-isotropic distribution of electron pitch angles, or to differential Doppler boosting of a relativistic jet/counterjet pair. With a suitably chosen pitch angle distribution, one can make a jet all but invisible (e.g. Van Gronigen et al), but this seems contrived.

If two jets are intrinsically equal, but have an observed ratio R due to different Doppler enhancements, then

$$\left(\frac{1+\beta\cos\theta}{1-\beta\cos\theta}\right)^{2-\alpha} = R$$

where θ is the angle between the jet and the line of sight.

$$\beta = \frac{R^{\frac{1}{2-\alpha}} - 1}{\cos\theta\left(R^{\frac{1}{2-\alpha}} + 1\right)}$$

The condition $\beta<1$ yields

$$\theta < \cos^{-1}\left[\frac{R^{\frac{1}{2-\alpha}} - 1}{R^{\frac{1}{2-\alpha}} + 1}\right]$$

$$\cos\theta_{max} = \beta_{min}$$

Table 1 gives θ_{max}, β_{min}, and γ_{min} for the values of R quoted in Chapter 1 (a spectral index of -.5 has been assumed); the R=100 entry demonstrates what could be achieved with suggested VLBI

arrays. Note that the values of R quoted in Chapter 1 are lower limits; the angles in Table 1 are thus strong upper limits and the values of β and γ lower limits. At $\theta=\theta_{max}$, $\beta=1$; but for $\theta \lesssim \theta_{max}-10^{\circ}$, β remains roughly constant.

The constraints imposed by the values in Table 1 have particular significance for Cyg A. The lower limit to R of 15 (Chapter 1) implies that θ must be less than 60°, and is almost certainly less than 55° (or else a very large γ-factor would be required). This is in contrast to the value of $90^{\circ}\pm25^{\circ}$ given by Hargrave and Ryle (1974), based on the broad but sharp termination of the southern hot spot. They allow the possibility that the northern lobe has a lower inclination to the line of sight than does the southern lobe, but the high symmetry of this source makes such a possibility seem unlikely. It therefore seems nearly certain that in Cyg A the jet and counterjet must have intrinsic differences, the similarity of the two lobes notwithstanding. If the limit on R can be raised significantly by future, high-dynamic range VLBI observations, this conclusion could be strengthened.

III. PHYSICAL CONDITIONS FROM SYNCHROTRON THEORY

In this and the following section, the radio emission from the four sources observed in Chapter 1 will be assumed to be due to incoherent synchrotron radiation. With this radiation mechanism, and in the absence of bulk relativistic motion, the peak brightness temperature must be less than 10^{12} K. If it did exceed this value, the photon density would be so great that the electron cooling time due to Inverse Compton radiation would be very short. In Table 2 the peak brightness temperatures of the four sources for each epoch are given. Models of the brightness distribution consisting of two or three gaussian components were used for these calculations. In those cases where the model-fitting procedure assigned a dimension of $<.2\ \lambda/d$ to a gaussian component, that dimension was increased to $.2\ \lambda/d$ for the brightness temperature calculation.

The peak brightness temperatures range from 1.8×10^{10} K to 7.0×10^{10} K. In no case are they large enough to be in conflict with inverse Compton lifetimes. For weak sources such as these, earth-based observations are insufficient to detect brightness temperatures as large as 10^{12} K.

To determine the physical conditions inside these sources, a power law spectrum has been assumed. Actually, this is terminated at some frequency by synchrotron self-absorption, but this does not affect the following calculations of U_{min} and B_{eq}. The energy in

relativistic electrons is

$$U_e \propto L B^{-1.5} f(\nu_1, \nu_2, \alpha),$$

where L is the synchrotron luminosity (neglecting self-absorption), B is the magnetic field, ν_1 and ν_2 are the minimum and maximum frequencies of the power-law spectrum, and α is the spectral index. f is a fairly weak function of ν_1, ν_2, and α. The values of ν_1, ν_2, and α assumed for each component of each source are listed in Table 3.

The energy in relativistic protons has been assumed by different people to be from 0 to 100 times that in relativistic electrons. A value of 0 has been assumed here, so that a firm lower limit on the total energy and pressure in the source can be calculated.

The total energy in particles and magnetic field is

$$U_{tot} = c_0 B^{-1.5} + c_1 B^2$$

Assuming equipartition (i.e. $U_{mag} = U_{particles}$) gives

$$B_{eq} = \left(\frac{c_0}{c_1}\right)^{2/7}$$

Varying B to minimize U_{tot} gives

$$U_{min} = .99\ U_{eq}$$

Varying B to minimize the pressure P gives

$P_{min}=.53\ \frac{U_{eq}}{V}$, where V is the component volume

Table 4 gives B_{eq}, U_{min}, and P_{min} for each component of each source. $H_0=50$ has been assumed. The values of B_{eq} are similar for each source; $B_{eq}\sim.1$ Gauss in the core, dropping to .01–.02 in the outer parts of the jet. The values of U_{min} are also similar from source to source, except for 0055+30. This source is at one third the distance of the other three; a given angular resolution therefore corresponds to a volume $\frac{1}{27}$ as great as in the other three. From the variation time scale in 3C 111 (a few years) and the values of U_{min} for the core components in Table 4, an energy input rate of $\sim 5 \times 10^{50}\ \frac{erg}{yr} \sim 3 \times 10^{-4}\ \frac{M_\odot}{yr}$ can be derived. This is well within the range that could be provided by a massive black hole. The jets have larger values of U_{min} than the cores, but they presumably accumulate their energy over a longer period of time.

Electrons radiating via synchrotron radiation have a half life $\tau_{syn}=\frac{16.1}{B^2\gamma}$ yr, where $\gamma\approx\left(\frac{\nu}{1.2 \times 10^6 B}\right)^{1/2}$

Values of τ_{syn} for $B=B_{eq}$ and $\nu=10.6$ GHz are given in Table 5. The electron lifetimes in the cores are not much longer than the light travel times across them, suggesting at least mildly relativistic outflow velocities. The electron lifetimes in the jets are a few times longer than the light travel times from the core. This suggests relativistic jet velocities, but does not require reacceleration within the jets.

Most compact radio sources are observed to be self-absorbed at low frequencies. The observations of Chapter 1 are at only one frequency, and therefore cannot be used to obtain spectral information. However, the optical depth can be estimated from the equipartition magnetic field.

$$\kappa_\nu \propto N_0 B^{1.5-2\alpha} \left(\frac{\nu}{1.25 \times 10^{19}}\right)^{\alpha-2.5}$$

where the spatial density of relativistic particles is $N_0 E^{2\alpha-1}$ (N_0 can be calculated from the observed luminosity).

In Table 5, the calculated optical depths at 10.6 GHz, and the frequencies at which $\tau=1$ are given. These values are for homogeneous components whose dimensions are the FWHM of the gaussian models. Because of this, the sources will start showing optical depth effects at frequencies higher than predicted by these calculations. ($\tau_\nu \propto \theta^{-2}$, where θ is the angular size assumed for the source)

IV. PRESSURE CONFINEMENT OF THE JET IN CYGNUS A

If the jets in these sources are confined by thermal pressure, then the pressure in surrounding medium must be greater than the value of P_{min} calculated in part III.

$$nkT > P_{min}$$

$$(1) \quad n_e T > \frac{P_{min}}{1.95k}$$

Additional constraints are possible (Readhead et al 1978). Cyg A will be the only source discussed here; it was chosen because of its historical interest and because an excellent upper limit to its nuclear X-ray flux exists. In the following calculations, a spherically symmetric gas cloud centered on the core has been assumed. The 1978.93 Cyg A observations have been chosen because they have a higher dynamic range than the 1979.44 observations.

The source model of Cyg A for 1978.93 accounts for over 80% of the flux of the central component. The optical depth at 10.6 GHz of the surrounding gas cloud must therefore be less than 0.2. For free-free absorption, this is not a significant constraint, but for Compton scattering it is:

$$(2) \quad n_e < \frac{.2}{\sigma R} \ ,$$

where R is the cloud radius (equal to the length of the jet component being considered). Induced Compton scattering (Wilson 1978) will be significant at these brightness temperatures, but it will result in photons being scattered within the beam (not into or out of it). It changes equation (2) by only a small (<2) factor, and has therefore not been included.

From HEAO-A X-ray observations, preliminary results indicate that the flux from a point source centered on the core of Cyg A is less than 10^{42} erg/sec in the .5-4.5 keV band (Ethan Schreier, private communication). Assuming this to be from thermal bremsstrahlung yields the following constraint

$$(3)\quad n_e < \sqrt{\frac{10^{42}}{1.4 \times 10^{-23} \langle \sum_i Z_i \frac{n_i}{n_e} \bar{g}_{ff_i} \rangle T_8^{1/2} \frac{4}{3}\pi R^3 \left[e^{-\frac{.058}{T_8}} - e^{-\frac{.52}{T_8}} \right]}}$$

A fourth constraint is imposed by bremsstrahlung cooling. The total free-free emissivity per unit volume is

$$4\pi \int j_\nu \, d\nu \approx 1.4 \times 10^{-27} \, T^{.5} n_e^{\,2}$$

$$\tau_{cool} \sim \frac{10^4 T^{.5}}{n_e} \text{ yr}$$

It is of interest to equate this to a heating time. The radiative

heating time from the central source is $\sim \frac{U_{thermal}}{L_{nonthermal}\,\tau_{ff}}$, which is very long for frequencies above the self-absorption cutoff and values of n_e and T not already excluded by other processes. Mechanical heating will probably dominate. The heating time for this is not so obvious. An upper limit, given sufficient energy input, is the sound speed crossing time,

$$\tau_{heat} \sim \frac{R}{c_s} \sim \frac{R}{10^4 T^{.5}}$$

There will be some local mechanical heating on shorter time scales, but this will result in temperature inhomogeneities, significantly increasing the emission measure. The X-ray observations would then be an even stronger constraint. To account for some local heating, a more conservative estimate of the heating time can be chosen:

$$\tau_{heat} = \frac{R}{3c_s}$$

The condition $\tau_{heat} < \tau_{cool}$ leads to

$$(4) \quad n_e < \frac{10^{12} T}{R}$$

The constraints imposed by equations (1)-(4) on the outer jet component of Cyg A are shown in Figure 1. If the jet is pressure confined, T must be greater than 2×10^9 K.

In the absence of a massive black hole in the center of Cyg A, the nuclear potential could not confine a gas with $T \gtrsim 10^8$ K. However, there is quite possibly a black hole powering the radio source; this would dominate the potential at the distance of the jet. Requiring gas at $\frac{R}{2}$ to be bound by the potential of the hole gives (for the outer jet component)

(5) $T \lesssim 7 \times 10^7 M_9$,

where $M_9 = \frac{M_{hole}}{10^9 M_\odot}$

If a gas at 2×10^9 K is to be bound, then $M_9 \gtrsim 30$. Therefore, unless there is a black hole with $M \gtrsim 3 \times 10^{10} M_\odot$ in the center of Cyg A, the observed msec jet is very unlikely to be pressure confined. If there were a large outflow of gas from the core, this constraint would not apply, but this outflow gas would have to be hotter than 10^9 K.

If the jet is not confined by external pressure, it is either self-confined by its own magnetic field, or is a free jet. If it is freely expanding, the observations of Chapter 1 indicate a full opening angle $\xi \lesssim 10°$, implying a Mach number $\mathcal{M} \gtrsim 6$. In the absence of non-relativistic jet material, this implies a large jet γ-factor ($\gamma > \sqrt{19}$).

V. CONCLUSIONS

Four sources, chosen for their large scale symmetry, all have strong small scale asymmetry. In all four cases, this is probably due to an intrinsic asymmetry, rather than to geometrical or radiative effects. The model of two identical but oppositely directed jets (Blandford and Rees, 1978) does not apply to these sources.

Physical arguments based on synchrotron theory show that these sources must have at least weakly relativistic core outflow and jet velocities. The jet in Cyg A (the best studied of the four sources) is almost certainly not confined by external pressure. A better measurement of its width at various distances from the core could help ascertain whether or not it is a free jet. If it is not, it may be self-confined by magnetic pressure.

REFERENCES

Blandford, R. D., and Rees, M. J. 1974, M.N.R.A.S., 169, 395.

Hargrave, P. J., and Ryle, M. 1974, M.N.R.A.S., 166, 305.

Lonsdale, Colin 1981, Ph. D Thesis, University of Manchester.

Readhead, A. C. S., Cohen, M. H., and Blandford, R. D. 1978, Nature, 272, 131.

Van Gronigen, E., Miley, G. K., and Norman, C. A. 1980, ANA, 90, L7.

Wilson, D. B. 1978, M.N.R.A.S., 185, 297.

Table 1

Jet Angles and Velocities

R	θ_{max}	β_{min}	γ_{min}
8	66.8°	.394	1.09
15	60.4°	.495	1.15
100	43.4°	.726	1.46

Table 2

Peak Brightness Temperatures

Source	Epoch	Maximum T_b
3C 111	1978.93	7.0×10^{10}
3C 390.3	1978.93	4.1×10^{10}
3C 390.3	1979.75	5.3×10^{10}
Cyg A	1978.93	2.7×10^{10}
Cyg A	1979.44	3.4×10^{10}
0055+30	1978.93	2.8×10^{10}
0055+30	1979.44	1.8×10^{10}

Table 3

Model Parameters

Source	Epoch	Component	$S_{10.6}$ (Jy)	AX[1] (msec)	AY[2]	ν_1 (GHz)	ν_2 (GHz)	α
3C 111	1978.93	core	1.08	.55	.3	.01	300.	-.3
		inner jet	.41	2.55	.3	.01	50.	-.6
		outer jet	.37	7.7	2.	.01	20.	-.6
3C 390.3	1978.93	core-jet	.45	.65	.18	.01	300.	-.3
		halo	.05	2.4	2.3	.01	50.	-.6
3C 390.3	1979.75	core	.41	.59	.14	.01	300.	-.3
		jet	.03	1.1	.10	.01	50.	-.6
Cyg A	1978.93	core	.51	.84	.24	.01	300.	-.3
		inner jet	.26	1.52	.60	.01	50.	-.6
		outer jet	.21	11.2	.77	.01	20.	-.6
Cyg A	1979.44	core	.38	.52	.23	.01	300.	-.3
		inner jet	.26	.71	.16	.01	100.	-.6
		outer jet	.18	2.0	1.0	.01	50.	-.6
0055+30	1978.93	core	.42	.89	.18	.01	300.	-.3
		inner jet	.23	3.5	.35	.01	50.	-.6
		outer jet	.15	8.2	4.4	.01	20.	-.6
0055+30	1979.44	core	.25	.66	.24	.01	300.	-.3
		inner jet	.25	1.8	.39	.01	50.	-.6
		outer jet	.15	5.7	.49	.01	20.	-.6

[1] AX is the FWHM along the major axis of the elliptical gaussian component

[2] AY is the FWHM along the minor axis of the elliptical gaussian component

Table 4

Derived Physical Parameters

Source	Epoch	Component	B_{eq}	U_{min}	P_{min}
3C 111	1978.93	core	.11	2.8×10^{51}	5.1×10^{-4}
		inner jet	.066	3.5×10^{51}	1.9×10^{-4}
		outer jet	.015	2.5×10^{52}	9.5×10^{-6}
3C 390.3	1978.93	core-jet	.10	2.0×10^{51}	4.2×10^{-4}
		halo	.011	7.3×10^{51}	5.1×10^{-6}
3C 390.3	1979.75	core	.11	1.3×10^{51}	4.9×10^{-4}
		jet	.071	2.6×10^{50}	2.1×10^{-4}
Cyg A	1978.93	core	.081	2.8×10^{51}	2.8×10^{-4}
		inner jet	.043	4.9×10^{51}	7.9×10^{-5}
		outer jet	.020	1.2×10^{52}	1.6×10^{-5}
Cyg A	1979.44	core	.091	1.7×10^{51}	3.5×10^{-4}
		inner jet	.11	1.1×10^{51}	5.3×10^{-4}
		outer jet	.027	7.0×10^{51}	3.1×10^{-5}
0055+30	1978.93	core	.12	1.3×10^{50}	6.3×10^{-4}
		inner jet	.063	2.4×10^{50}	1.7×10^{-4}
		outer jet	.010	2.2×10^{51}	4.2×10^{-6}
0055+30	1979.44	core	.10	8.8×10^{49}	4.2×10^{-4}
		inner jet	.072	2.1×10^{50}	2.2×10^{-4}
		outer jet	.039	2.9×10^{50}	6.4×10^{-5}

Table 5

Lifetimes and Optical Depths

Source	Epoch	Component	τ_{syn} (yr)	Optical Depth $\tau_{10.6}$	$\nu(\tau=1)$ (GHz)
3C 111	1978.93	core	5	.05	3.6
		inner jet	10	.004	1.8
		outer jet	90	.00008	.5
3C 390.3	1978.93	core-jet	5	.03	2.9
		halo	100	.00003	.4
3C 390.3	1979.75	core	5	.04	3.2
		jet	9	.002	1.5
Cyg A	1978.93	core	7	.02	2.4
		inner jet	20	.002	1.4
		outer jet	60	.0001	.6
Cyg A	1979.44	core	6	.02	2.6
		inner jet	5	.02	3.1
		outer jet	40	.0005	.9
0055+30	1978.93	core	4	.02	2.7
		inner jet	10	.001	1.3
		outer jet	200	.00001	.3
0055+30	1979.44	core	5	.01	2.1
		inner jet	9	.003	1.6
		outer jet	20	.0003	.8

Figure 1

Cyg A 1978.93 Outer Jet Component

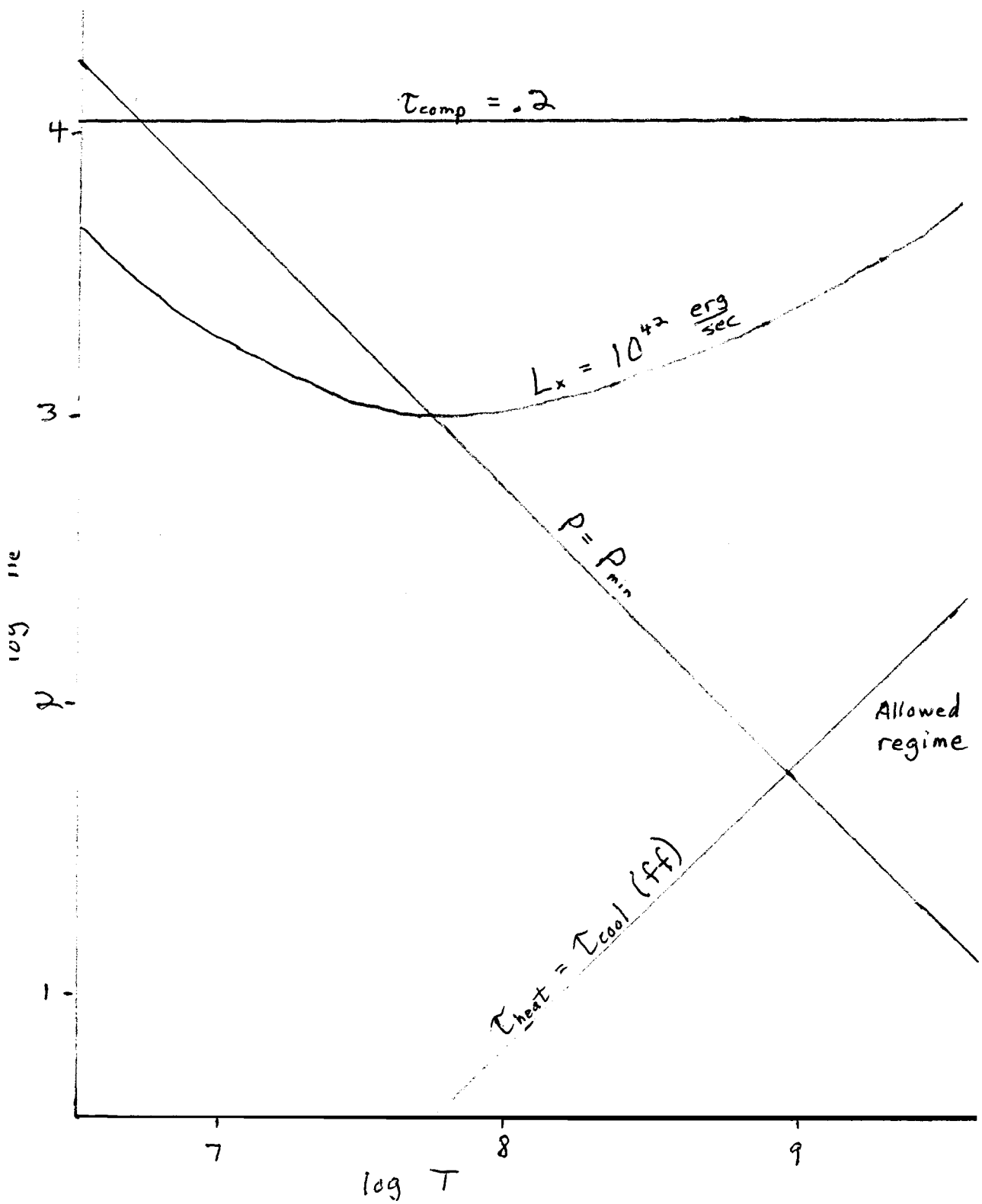

CHAPTER 3

A PRECESSING JET MODEL OF COMPACT RADIO SOURCES

ABSTRACT

An attempt is made to explain the structure of compact radio sources with a precession-like motion of a relativistic jet. It is found that the curvature of these sources can be readily explained in this way. In addition, the knots which are often revealed by VLBI observations arise naturally in such a model. The main problem with the model is that it cannot by itself explain the arcsecond structure of asymmetric radio sources.

I. INTRODUCTION

Many extragalactic radio sources fall into one of two categories: symmetric and asymmetric (Readhead et al 1978). Symmetric sources typically have a large (up to several Mpc) overall projected size on the sky, and show little or no change in position angle from their innermost structure to their kpc scale structure (head-tail sources show curvature farther out). Asymmetric sources have a strong, very asymmetric core (Readhead et al, 1979), and a small (generally a few tens of kpc or less) projected size on the sky. They generally show curvature of 20°-40° from the nucleus to their outer structure. This has been interpreted by Readhead et al (1978) as a consequence of different angles between a relativistic jet and the line of sight. In this scheme, all jets are assumed to

be slightly curved - asymmetric sources show a much larger curvature because of projection effects. The intrinsic curvature of these jets could be due to a flow along a fixed, curved path, or to a motion of the source of the jet. This paper deals with one of the two general types of jet motion - rotation. Precession has been chosen for study because it is well-defined and easy to calculate. However, except in the special case of SS433 (Abell and Margon 1979), the jet's motion is probably more complicated. Translational motion of a jet may be important in some sources, e.g. 3C 31 (Blandford and Icke, 1978) and 3C 449, but will not be covered here.

The precession model is described in Section II. Section III explains the choice of parameters, and Section IV presents some results. Conclusions are given in Section V.

II. THE MODEL

In this model, a special case of the one proposed by Blandford and Königl (1979), a jet and an identical counterjet are ejecting material smoothly at a constant relativistic velocity βc. The jet (and counterjet) precess at a constant rate $\frac{2\pi}{\tau}$ around a cone, with a cone half-angle of ψ. The cone axis makes an angle θ_o to the line of sight. The emissivity per unit length is assumed to decay as a power of the distance ($\varepsilon \propto r^{-k}$) from the core, corresponding to an optically thin jet. At a distance R_{min} from its source, the jet becomes optically thin at the emitted frequency - for $R<R_{min}$ the jet has a self-absorbed spectrum, and its intensity drops off sharply towards smaller R. This optically thick core is a prominent feature on VLBI maps. Over the range of emitted frequencies spanned by the jet's precession cycle (a constant observing frequency is assumed), R_{min} is assumed to vary as $1/\gamma_{emitted}$. This has an interesting consequence in the implied jet/counterjet flux ratio. For a stationary jet,

$S_{tot} \propto R_{min}^{1-k}$

(1) $R_{min}(\text{counterjet}) = \mathcal{D}^{2-\alpha} R_{min}(\text{jet})$

($\mathcal{D}$ is the Doppler factor for the jet),

(2) $S_{tot}(\text{counterjet}) = \mathcal{D}^{-2(2-\alpha)} \mathcal{D}^{-2(3-k)} S_{tot}(\text{jet})$

$= \mathcal{D}^{-2+2\alpha+2(k-4)} S_{tot}(\text{jet})$,

compared to the canonical

(3) $S_{tot}(\text{counterjet}) = \mathcal{D}^{-4+2\alpha} S_{tot}(\text{jet})$.

Essentially all of the counterjet's flux comes from $R<<R_{min}(\text{jet})$, and would therefore be part of the unresolved core in VLBI maps made

with earth-based arrays. However, for small γ ($\gamma \lesssim 2$), it would reduce the shift of the position of this core with observing frequency by a measurable amount.

Most of the flux from the source arises from the region near R_{min}. Thus, the integrated spectrum is very sensitive to the variation of optical depth and emissivity through this region. However, no effort has been made to fit observed source spectra by adjusting the behavior of these properties.

At frequent intervals in the precession cycle, the path of the jet and counterjet (taking time delay effects across the source into account), as well as the intensity per unit length (projected onto the sky) were calculated. For the intensity calculations, an enhancement of $\mathcal{D}^{3-\alpha}$ over the emissivity in the rest frame of the material has been assumed. ($\mathcal{D}=[\gamma(1-\beta\cos\theta)]^{-1}$ and α=d ln S/d ln ν; θ is the angle between the direction of emission and the line of sight.) The jet (and counterjet) were convolved with a circular gaussian to simulate VLBI maps. The jet was assumed to be unresolved perpendicular to its length (as observations indicate). This implies that the opening angle $\xi < 10^{\circ} \sin\theta_o$. Since $\gamma^{-1} \sim \sin\theta_o$ (as discussed in section III), $\xi \lesssim \frac{1}{6\gamma}$. $\xi \sim 1/\mathcal{M}$, where $\mathcal{M}$ is the Mach number of the flow. Therefore $\mathcal{M} \gtrsim 6\gamma$, which is easily satisfied for a non-relativistic fluid ($\mathcal{M} = \frac{\gamma\beta}{\beta_s}$ if $\mathcal{M} \equiv \frac{v}{c_s}$, Königl 1980), but not for a relativistic one ($\mathcal{M} \approx \gamma\beta\sqrt{2}$).

III. CHOICE OF JET PARAMETERS

In order to restrict the region in parameter space to investigate, a source luminosity function (in both intrinsic flux, S_0, and jet γ-factor, $\gamma=1/\sqrt{1-\beta^2}$) was selected, and the distribution in viewing angle for the range of observed flux, S, and γ was calculated. The luminosity function chosen was $dN=S_0^{-b-1}\gamma^{-\delta}e^{-\frac{\gamma}{\gamma_c}}$ (i.e. a power law in γ, with an exponential cutoff to prevent very large ($\gtrsim$100) values of γ from contributing).

b was chosen to be 1.5, consistent with results obtained from source counts (e.g. Wall *et al*, 1981). A flat spectal index (α=0.) was used, consistent with the overall spectra of most compact sources. δ and γ_c were chosen to satisfy two criteria. 1) A substantial fraction ($\gtrsim$30%) of the sources at a given S should have $\gamma<2$. This is necessary, because the central components of a large number of symmetric sources, whose jets should be nearly in the plane of the sky, are visible. 2) A nonnegligible fraction should have $\beta_{obs}>7$ ($\beta_{obs}=\beta\sin\theta/(1-\beta\cos\theta)$), since this is the value recently measured for 3C 273 from VLBI observations (Pearson *et al*, 1981). (They calculate a different value of β_{obs} due to a different value of H_0; H_0=75 and q_0=.05 are assumed in this paper). Typical values of δ and γ_c which satisfy these criteria are δ=1.8 and γ_c=10, but a fairly wide range of values is allowed.

The very different Doppler boosting for different viewing angles has been used by Scheuer and Readhead (1979) to explain the large range in the ratio of radio to optical flux from quasars. Recent radio surveys of optically selected quasars (Strittmatter et al, 1980 and Condon et al, 1981) imply that other factors besides geometry contribute to this ratio. However, several features of compact radio sources are well explained by the simple geometric model, and it has been used here.

Because the distribution in γ is independent of S_0, the distribution in γ and θ is the same for all S. Two things are readily apparent in the results. First, the mean of the distribution in γ is larger for fixed S than for fixed S_0. (i.e. The sources one sees are biased towards those with large γ). Second, most observed sources have θ between $.3\gamma^{-1}$ and γ^{-1}, with the peak occurring $\sim.8\gamma^{-1}$ (except for $\gamma<2$, for which $\langle\theta\rangle$ $\sim.9\text{-}1.1\gamma^{-1}$). The average β_{obs} is $.8\gamma\beta$ for all γ. Therefore, if superluminal expansion with apparent velocity β_{obs} is seen in a source, a γ-factor of only $\sim1.3\ \beta_{obs}$ is implied. These results apply even for rather different luminosity functions.

For parameters, values of θ_o between $.4\ \gamma^{-1}$ and γ^{-1} were used. The precession angle ψ was chosen to be 1° or 2°. The spectral index for the optically thin part of the jet was taken to be $-.6$. Values of γ ranging from 1.2 to 15 were used. The period of precession was varied from values so long that no curvature would be seen over the size range covered by VLBI observations to values so short that curvature in several directions would be visible. The

intermediate case, moderate to large curvature in one direction, was studied the most, since that is what is observed in compact asymmetric extragalactic sources. The value of τ that produces this depends on the radius at which the jet becomes optically thin. If the observed radius for which the jet becomes optically thin is 5 pc (1 msec at z=.5), k~2.2, and $\theta_o = .8\gamma^{-1}$, then τ~1000 yrs, roughly independent of γ. These values produce a bend of approximately $\frac{\psi}{\theta_c}$ in 50 msec, as observed in 3C 273. If the observed R_{min} ($=R_{min}\ \sin\theta$) is independent of γ, $R_{min} \propto \gamma$. This is physically reasonable, since $\nu_{em} \propto \gamma^{-1}$, and $R_{min} \propto 1/\nu_{em} \propto \gamma$. Values of k (the coefficient of emissivity per unit length) between 2 and 2.5 were used in all the models, consistent with VLBI observations of 3C 273 and 3C 345 (Readhead et al, 1979 and Wilkinson et al, 1979). For comparison, $k=1-7\alpha/3=2.4$ for adiabatic loss of particle energy, $B \propto R^{-1}$, and no radiative losses. For the jet flux to be finite, k must be greater than 1.

IV. RESULTS

The range of parameters that were used yielded a wide variety of simulated source shapes. Three typical ones, which resemble VLBI maps of 3C 345, are shown in figure 1. Note that if the precession period were a factor of 5 greater, very little curvature would be seen; if it were a factor of 5 less, several bends would be present. The source curvature is greatly reduced during certain phases of the precession cycle; this straightening out may have been seen in the innermost part of 3C 273 (Pearson et al, 1981), but not in 3C 345.

The jet's position angle varies during the cycle. This has not been seen in extragalactic sources, but VLBI observations have been made for only a very small fraction (~.01) of the assumed precession period of 1000 years. Because it is precessing, the jet does not have its flux boosted by precisely $\mathcal{D}^{2-\alpha}$. However, the precession considered here is sufficiently slow that the jet's flux is always within 10% of $S_0 \mathcal{D}^{2-\alpha}$ ($\mathcal{D}$ is the Doppler factor at the base of the jet), so that the effect is too small to significantly change the observed luminosity function.

With many (though not all) choices of parameters, hot spots (regions of enhanced emission) appear in the models. They are up to 8 times brighter than the surrounding regions of the jet, and maintain their identity for from one to many precession periods (depending upon the parameters). They result from a 'piling up' of material along the line, rather than from an increased Doppler enhancement during part of the precession cycle. This latter effect causes very broad regions of enhanced emission, and generally becomes noticeable only when γ is at least 4-5; the hot spots are relatively small (sometimes very small) in extent, and occur with all values of γ. Figure 2 shows a jet with a hot spot moving outwards superluminally.

To see why hot spots form, consider the time variations in β_{obs}. The maximum possible β_{obs} occurs for $\theta = \cos^{-1}\beta$. When θ is changing towards $\cos^{-1}\beta$, β_{obs} increases, and ejected material tends to catch up with material ejected earlier. If ϕ (the angle in the plane of the sky) is nearly constant during this time, the

material will pile up more or less along the line of sight, forming a hot spot. ϕ is slowly varying only near the edges of the precession cone; this is where hot spots form. If $|\theta_o - \cos^{-1}\beta| > \psi$ (the usual case, given the small values of ψ used here), then hot spots will form only on one side of the precession cone. If $|\theta_o - \cos^{-1}\beta| < \psi$, hot spots can form on both sides, but those on one or both sides are very weak. If β_{obs} varies slowly with time, the material will bunch up a long distance from the core; the hot spots will sharpen as they move out, and will last a long time. This is generally the case for low $\gamma(\lesssim 2)$, since $\frac{\partial \beta_{obs}}{\partial \theta}$ is small. These long-lived hot spots have been seen in in SS433 (Hjellming and Johnston 1980). For larger $\gamma(\gtrsim 4)$, $\frac{\partial \beta_{obs}}{\partial \theta}$ is larger and β_{obs} changes rapidly with time; in such a case the hot spots will form near the core, remain sharp for a precession period or less, and then begin to disperse. (From another view, if a hot spot is sharp at one epoch, it disperses both forwards and backwards in time at a rate proportional to the dispersion in β_{obs} of the material comprising it.) In both cases, the motion of the hotspots is very nearly rectilinear, with both β_{obs} and ϕ retaining almost the same values for as long as the hot spot is visible.

Although the hot spot motion on the sky is rectilinear, the motion of a hot spot in a compact radio source would not be observed to be precisely rectilinear. This is because one measures relative positions, not absolute positions, from VLBI maps. The position of the unresolved core on a VLBI map of a jet corresponds approximately to the point where the jet becomes optically thin ($R=R_{min}$); this point traces out a loop on the sky during a precession cycle. During

the interval $\tau/100$ (~10 years) after a hot spot first appears in these models, its measured β_{obs} varies by .2% - 1.5% and its measured PA varies by .02°-.8°. The magnitudes and signs of these changes depend on the parameters used, but in those cases where hot spots form near the core, the intial change in β_{obs} is an acceleration. These changes would be very difficult to detect observationally, and any deviation from a purely precessional motion of the jet's nozzle would further increase the difficulty of measurement. During the course of an entire precession period, the measured β_{obs} varies by $\sim\pm$10% and the measured PA varies by several degrees.

The above-mentioned properties of these hotspots are rather insensitive to the value of k. Increasing ψ causes β_{obs} to vary more rapidly; the hot spots then form more quickly and die out sooner. However, hot spots will form with a wide range (more than an order of magnitude) of ψ values.

The conditions that give rise to hot spots also cause the path traced out by the jet to bend sharply. Therefore, the knots in the jet of 3C 147 (Wilkinson *et al*, 1977) are not caused by this mechanism. The correlation between sharpness of hot spot and sharpness of curvature is very high. Any sharp bend in a jet resulting from precession will have enhanced intensity (always by at least 30% - usually by a factor of 2 or more). The radio jet of the quasar 4C 32.69 has two sharp bends, around which the intensity remains constant (Potash and Wardle, 1980). Van Gronigen *et al* (1980) use this to argue that the jet cannot consist of a

relativistic flow through a fixed, curved path. The constant intensity around the bends also implies that the bends cannot be caused by a precession-like motion of the jet nozzle, regardless of the jet velocity. The most likely explanation for the bends is a translation of the nozzle perpendicular to the direction of the jet flow (e.g. due to a close encounter between the quasar and a companion object).

The sharp bend present at a hot spot in this model has not been seen in any extragalactic source. This may be due to limited resolution (the hot spot spends most of its time in parts of the jet where it can be seen only by low frequency arrays).

Hot spots, or knots, are observed in many sources, and in at least two sources, 3C 273 (Pearson et al, 1981) and 3C 120 (Walker et al, 1981), these knots have been observed to move outward rectilinearly through the jet. Such knots have often been explained as clouds of gas or internal shocks that become entrained in the jet. In this paper, an alternative, purely kinematic explanation for them is given, one in which their rectilinear motion arises naturally. The main problem with explaining knots in this way is that only one hot spot (knot) is formed per precession cycle. 3C 273 has 3 or 4 knots within 50 pc of the nucleus, apparently all ejected within the last 15 years. Therefore, one must resort to more conventional knot origins, unless 1) the real motion of the source of the jet is much more complicated than precession, and produces several or many hot spots per 1000 year 'period', or 2) the random jitter at the base of the jet is accompanied by explosive events, which cause an uneven

flow in the jet. Quite possibly both mechanisms operate to some extent.

Counterjets are not prominent in the maps made from this model, since at a distance $R \gtrsim R_{min}(jet)$ from the core, the jet/counterjet flux ratio $\sim\gamma^{4-2\alpha}$. For $\gamma \lesssim 2$, the counterjet would be visible with currently achievable dynamic range, though for symmetric sources, where γ is probably this small, no msec counterjet is seen (Linfield 1981). Because of the different time dilation factors for the jet and counterjet, the counterjet is much more strongly curved than the jet, with $\frac{1+\beta\cos\theta}{1-\beta\cos\theta}$ times as many hot spots per unit length.

V. CONCLUSIONS

Precession can produce the curvature seen in asymmetric compact sources. It can provide a purely kinematic explanation for hot spots, moving out through a jet with superluminal velocities, such as is observed in 3C 273 (Pearson et al, 1981). Its prediction of a change in position angle with time is not in conflict with VLBI observations, because of their small time base. However, precession is in conflict with the narrow range of position angles exhibited by the arcsecond structure in these sources (e.g. the large jet in 3C 273). At the very least, therefore, other factors are influencing the direction of material flow on a scale of kpc. Such collimation is in fact observed in SS 433, where the bulge in W 50 (Geldzahler et al 1980) subtends a smaller angle at the core than the angle of the precession cone at the core (Niell et al 1981). In the NGC 315 jet

there is evidence for substantial collimation on a scale of a few kpc. (Willis et al 1981)

If the curvature in asymmetric sources is indeed produced by a motion of the jet's source, that motion is unlikely to be a pure precession. The precession periods required (~1000 years) are too short to be easily explained via known mechanisms. Periods that short are unlikely to occur with binary black holes (Begelman, Blandford, and Rees 1980), unless one assumes very low masses ($<10^4$ $M_\odot$) for the black holes. Such low mass holes are probably inadequate to power a radio source such as 3C 273. A more likely situation is an irregular motion of the rotation axis of an accretion disk (caused by stochastic events in the surrounding accretion disk, such as infall of either stars or interstellar gas clouds.)

If large scale jets (e.g. those in NGC 6251 and NGC 315) should prove to be relativistic (this is currently thought to be unlikely), then this model could be used to explain their structures. Precession periods of 10^5–10^7 years would then be needed; these are fairly easy to explain.

I thank Roger Blandford for suggesting this project, and for much guidance along the way. Marshall Cohen and Vincent Icke provided helpful discussions. Tony Readhead provided a critical reading of an early draft of this manuscript. This research was

supported in part by NSF grant AST 79-13249.

REFERENCES

Abell, G. O., and Margon, B. 1979, Nature, 279, 701.

Begelman, M. C., Blandford, R. D., and Rees, M. J. 1980, Nature, 287, 307.

Blandford, R. D., and Icke, V. 1978, M.N.R.A.S., 185, 527.

Blandford, R. D., and Königl, Arieh 1979, Ap. J., 232, 34.

Condon, J. J., O'Dell, S. L., Pushchell, J. J., and Stein, W. A., 1981 (preprint).

Geldzahler, B. J., Pauls, T., and Salter, C. J. 1980, ANA, 84, 237.

Hjellming, R. M., and Johnston, K. J. 1980, B.A.A.S., 12, 869.

Königl, Arieh 1980, Physics of Fluids, 23, 1083.

Linfield, Roger 1981, Ap. J., 244, 436.

Niell, A. E., Lockhart, T. G., and Preston, R. A. 1981 (submitted)

Pearson, T. J., Unwin, S. C., Cohen, M. H., Linfield, R. P., Readhead, A. C. S., Seielstad, G. A., Simon, R. S., and Walker, R. C. 1981, Nature (in press).

Potash, R. I., and Wardle, J. F. C. 1980, Ap. J., 239, 42.

Readhead, A. C. S., Cohen, M. H., and Pearson, T. J. 1978, Nature, 276, 768.

Readhead, A. C. S., Pearson, T. J., Cohen, M. H., Ewing, M. S., and Moffet, A. T. 1979, Ap. J., 231, 299.

Scheuer, P. A. G., and Readhead, A. C. S. 1979, Nature, 277, 182.

Strittmatter, P. A., Hill, P., Pauliny-Toth, I. I. K., Steppe, H., and Witzel, A. 1980, ANA, 88, L12.

Van Gronigen, E., Miley, G. K., and Norman, C. A. 1980, ANA, 90, L7.

Walker, R. C., Seielstad, G. A., Simon, R. S., Unwin, S. C., Cohen, M. H., Pearson, T. J., and Linfield, R. P. 1981 (submitted)

Wall, J. V., Pearson, T. J., and Longair, M. S. 1981, M.N.R.A.S., (in press)

Wilkinson, P. N., Readhead, A. C. S., Anderson, B., and Purcell, G. H. 1979, Ap. J., 232, 365.

Wilkinson, P. N., Readhead, A. C. S., Purcell, G. H., and Anderson, B. 1977, Nature, 209, 764.

Willis, A. G., Strom, R. G., Bridle, A. H., and Fomalont, E. B. (preprint)

FIGURE CAPTIONS

Figure 1

Simulated contour maps for 3 sets of parameters

a) γ=4 α=−.6 θ_o=6 ψ=2 k=2.2 A dynamic range of 30:1 has been assumed in making this map, so that it can be compared to current VLBI maps. The flux of this jet is boosted by a factor of 130 over the flux seen by a co-moving observer. The structure on the sky bends by 8° from the nucleus to the farthest point visible on this map; the intrinsic bend angle in the jet to that point is .75°.

b) The same map as in a), but with a dynamic range of 1000:1. This is more than can be achieved with current or suggested arrays, but a structure like this can be pieced together from observations at different frequencies (and therefore different resolutions), as has been done for 3C 273 and 3C 345 (Readhead et al 1978). Note the hot spot at the end of the jet. The PA change shown on this map is 37°, compared to an intrinsic bend angle of 4°. The scale on this figure is smaller than in a) - the horizontal bars in a) and b) represent the same distance on the sky. The contours in b) are more widely spaced than in a).

c) γ=10 α=−.6 θ_o=2 ψ=1 k=2.2 A dynamic range of 30:1 has been used here. The flux of this jet is boosted by a factor of 2100. Its PA change is 6.4°, compared to an intrinsic bend angle of 0.2°.

Figure 2

Jet with a hot spot. These 4 contour maps display the same jet at intervals of 20° in its precession cycle. The hot spot is moving outwards at an apparent speed ($\beta_{obs}c$) of 5.6 c. As it moves outwards, its flux decreases, but its contrast with its surroundings increases. The distance from the brightest part of the jet ($R \approx R_{min}$) to the hot spot is indicated. It increases nonlinearly with time because of the effect discussed in Section IV. The dynamic ranges of the four maps (the contour spacings are different on each map) are 100:1, 200:1, 300:1, and 500:1. For this jet, $\gamma=8$, $\alpha=-.6$, $\theta_o=4$, $\psi=2$, and $k=2$.

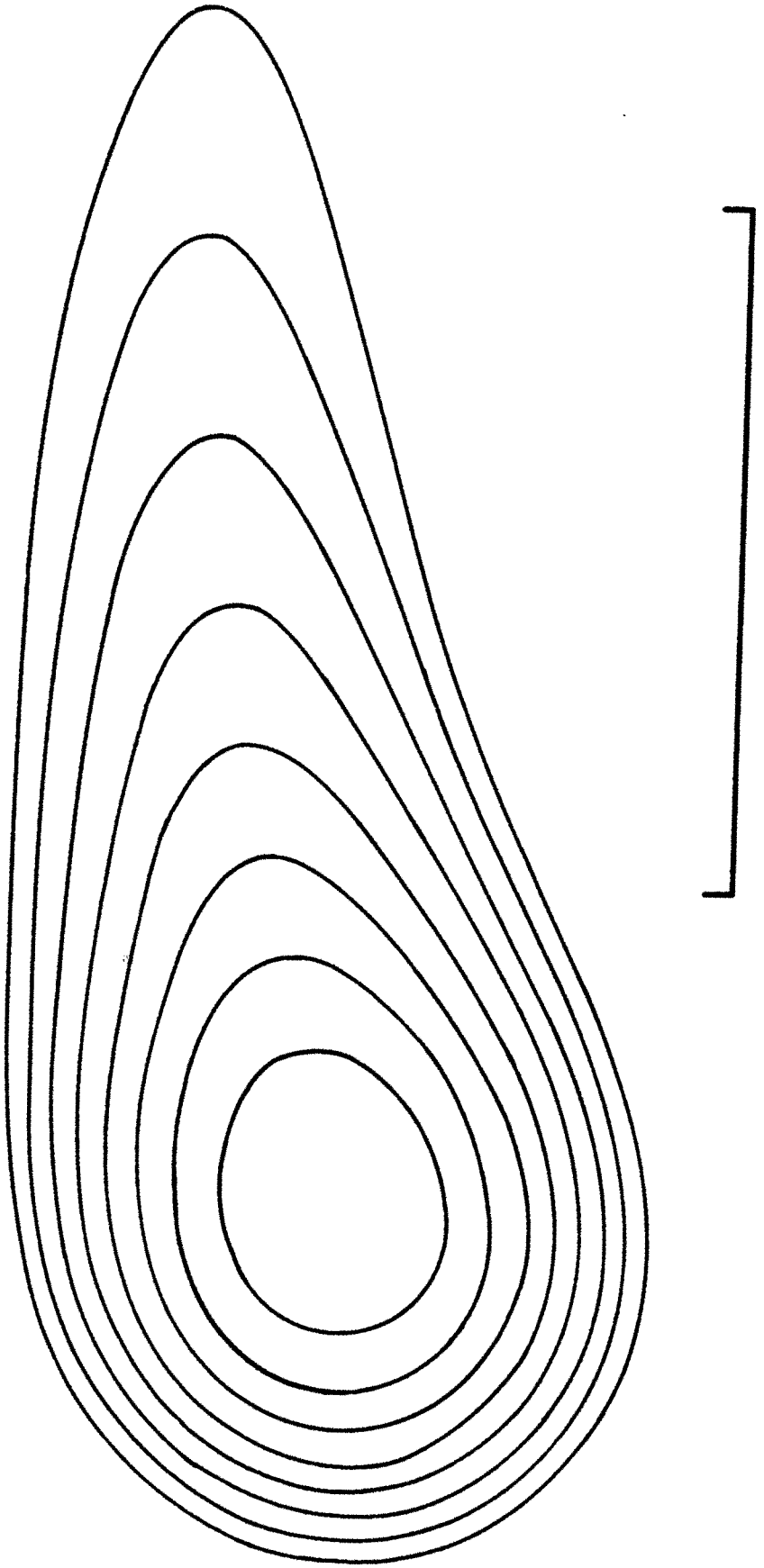

Figure 1a

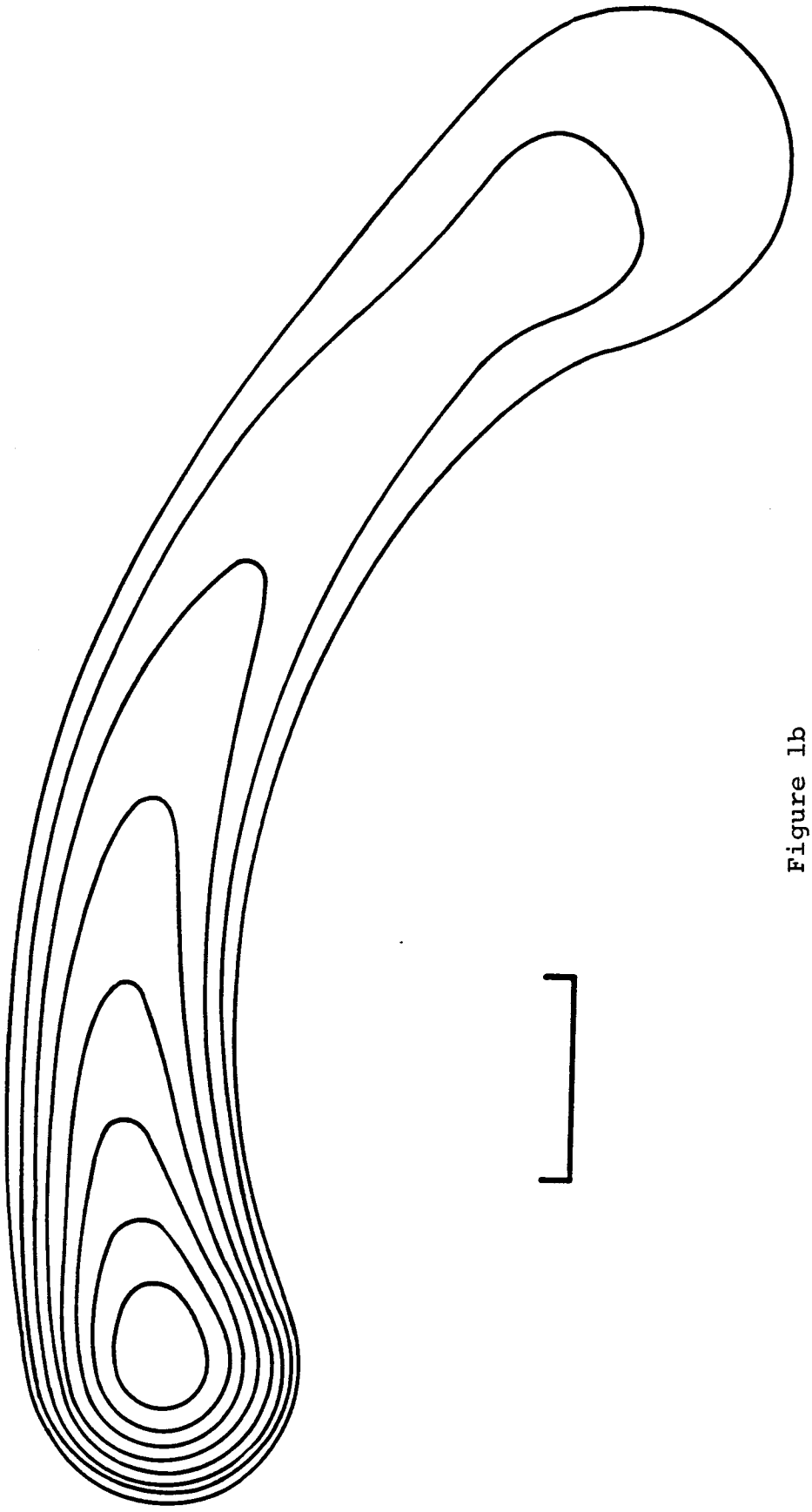

Figure 1b

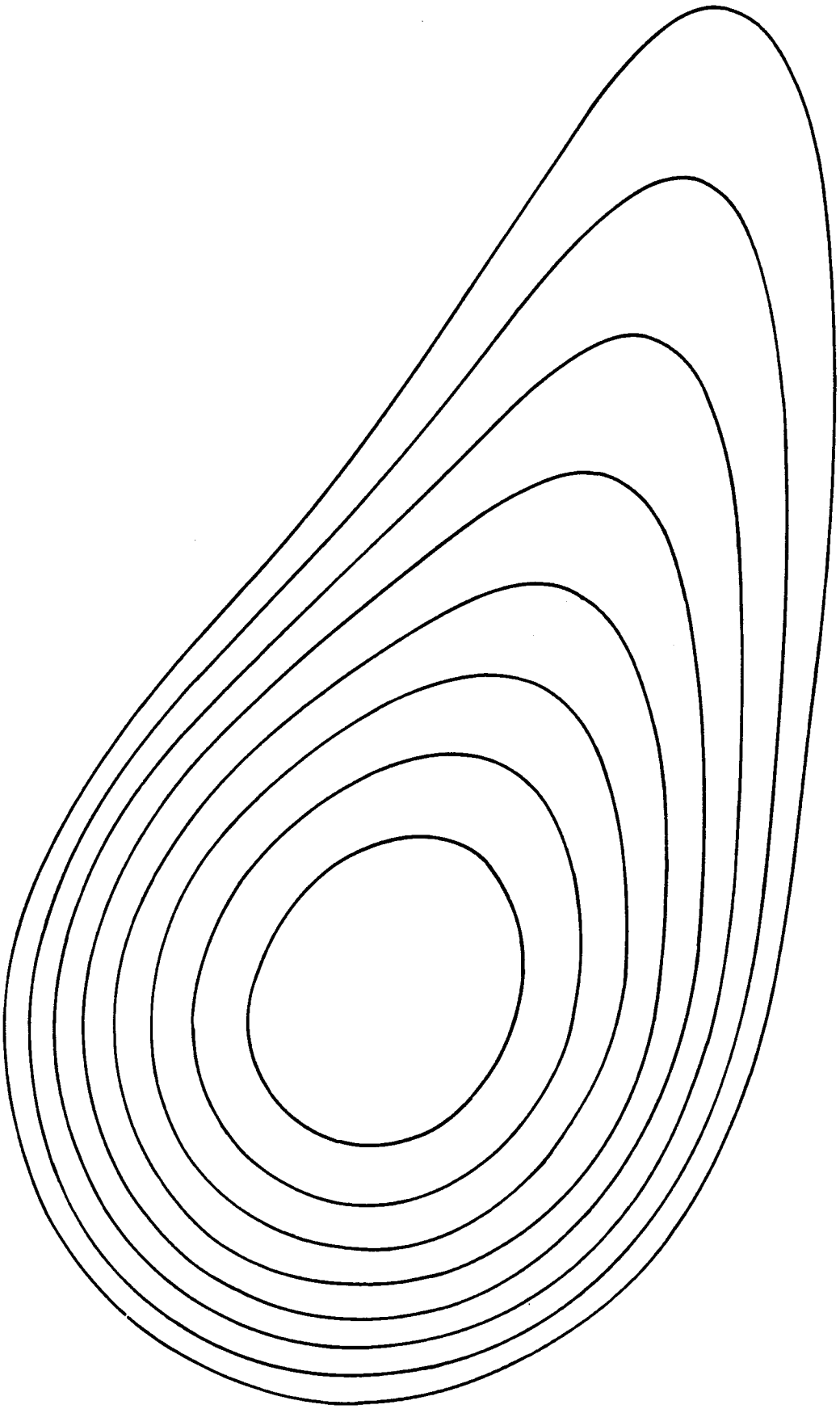

Figure 1c

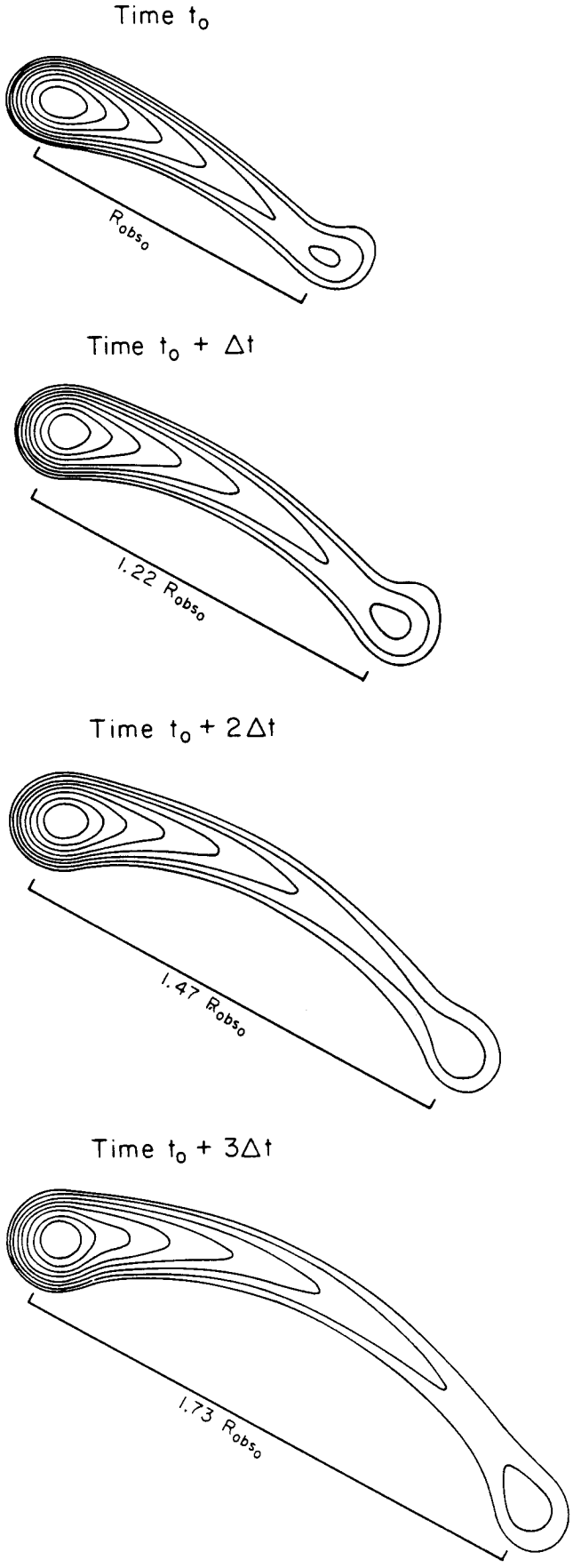
Time t_o
R_{obs_o}
Time $t_o + \Delta t$
1.22 R_{obs_o}
Time $t_o + 2\Delta t$
1.47 R_{obs_o}
Time $t_o + 3\Delta t$
1.73 R_{obs_o}

Figure 2